*J. Fluid Mech.* (1994), *vol.* 272, *pp.* 319–348



# A turbulent equilibrium boundary layer near separation

By PER EGIL SKÅRE AND PER-ÅGE KROGSTAD

Department of Mechanics, Thermo and Fluid Dynamics, Norwegian Institute of Technology, N-7034 Trondheim-NTH, Norway

(Received 24 June 1993 and in revised form 16 February 1994)

The experimental results for an equilibrium boundary layer in a strong adverse pressure gradient flow are reported. The measurements show that similarity in the mean flow and the turbulent stresses has been achieved over a substantial streamwise distance where the skin friction coefficient is kept at a low, constant level. Although the Reynolds stress distribution across the layer is entirely different from the flow at zero pressure gradient, the ratios between the different turbulent stress components were found to be similar, showing that the mechanism for distributing the turbulent energy between the different components remains unaffected by the mean flow pressure gradient. Close to the surface the gradient of the mixing length was found to increase from $\kappa_l \approx 0.41$ to $\kappa_l \approx 0.78$, almost twice as high as for the zero pressure gradient case. Similarity in the triple correlations was also found to be good. The correlations show that there is a considerable diffusion of turbulent energy from the central part of the boundary layer towards the wall. The diffusion mechanism is caused by a second peak in the turbulence production, located at $y/\delta \approx 0.45$. This production was for the present case almost as strong as the production found near the wall. The energy budget for the turbulent kinetic energy also shows that strong dissipation is not restricted to the wall region, but is significant for most of the layer.

## 1. Introduction

Turbulent flows subjected to strong adverse pressure gradients are frequently found to be a challenge to prediction methods (e.g. Wilcox 1993). In the report from the evaluation committee of the 1968 Stanford Conference on computation of turbulent boundary layers (Cockrell *et al.* 1968) the equilibrium boundary layer in a moderate adverse pressure gradient of Clauser (1954) was pointed out as being the flow giving the most trouble. If the strong gradient quickly leads to separation, the flow in this region is dominated by pressure effects and the modelling of the turbulence quantities in this region will not be critical for the overall boundary-layer results. However, the problem becomes more severe in flows which are affected by strong adverse pressure gradients acting over considerable streamwise distances. In such flows the choice of turbulence model may be quite essential for the predicted results.

The experiment to be reported here was initiated to provide more information about the terms that must be modelled in this type of flow. It was considered essential to produce a flow that was influenced by a strong adverse pressure gradient for a long streamwise distance for history effects to be important. From a computational point of view the equilibrium type of flow (defined in e.g. Clauser 1954 and Townsend 1976) appears attractive, since the profiles at different stations are similar when properly scaled, while the velocities in physical space may still undergo rapid streamwise

changes. Despite the experience from the 1968 Stanford Conference this should simplify the predictions. Equilibrium layers are also attractive when it comes to extracting information from the data. Once the similarity is established, gradients in the streamwise direction may be estimated with much higher precision than if the flow varies in a more random manner.

The simplest class of similarity boundary layers is the zero pressure gradient flow. However, according to Townsend (1976), this is not a true equilibrium flow since some of the requirements for complete similarity are that the skin friction coefficient, $C_f$, and the shape factor, $H$, should be constant. (See §3.1 for further discussions about similarity.) In the zero pressure gradient flow neither $C_f$ nor $H$ are constant, but decrease slowly downstream. Since the changes are very slow, the equilibrium conditions are approximately satisfied. To obtain constant skin friction the flow may either develop on a rough surface or be submitted to some well-defined pressure gradient. Some equilibrium experiments have been reported with streamwise pressure gradients, both favourable and adverse (e.g. Clauser 1954; Stratford 1959; Bradshaw 1967; East & Sawyer 1979). The main problem has been to maintain the equilibrium flow over a substantial streamwise distance when the adverse pressure gradient becomes significant. Clauser (1954) and East & Sawyer (1979) reported considerable problems in establishing their adverse pressure flows. Stratford (1959) on the other hand stated that he had no problems generating the much more sensitive flow of zero wall shear stress. Analysing pressure distribution 1 of Clauser (1954), Mellor & Gibson (1966) found that the non-dimensional pressure gradient parameter varied by 25% in the part of the flow claimed to be in equilibrium. Coles & Hirst (1968) found that the data indicate that the flow was slightly three-dimensional.

The data of Stratford (1959), taken on the curved surface used to generate the pressure gradient, appear to be dubious for a number of reasons. The inlet to the test section was only $8 \times 8$ in.$^2$ and with a boundary-layer thickness growing to about 4 in. the flow must have been affected, at least in the downstream end, by the poor aspect ratio. Stratford pointed out that secondary flows were likely to be present in the downstream half of the flow. Unfortunately this is the part of the flow where equilibrium appears to exist (zero wall shear stress and roughly constant shape factor). No information about the turbulence field is available for this flow since the measurements were obtained using Pitot tubes.

East & Sawyer (1979) reported measurements for seven different pressure distributions, four of which had adverse gradients. Only two of these (cases 4 and 7) reached a state of constant $C_f$ and $H$ for a short distance (of the order of two boundary-layer thicknesses). Since equilibrium was assumed to exist, measurements of mean velocity and turbulent stresses were only reported for one station for each case. Hence the documentation of similarity must be considered incomplete.

In the present study an equilibrium boundary layer was produced at high Reynolds numbers. A low, constant skin friction coefficient was obtained over a considerable streamwise distance. At the same time, the flow was kept sufficiently away from separation to allow conventional hot-wire measurements to be made with acceptable accuracy. To our knowledge only one equilibrium experiment exposed to a stronger pressure gradient has been reported (East & Sawyer, case 7), where detailed turbulence measurements have also been performed. Measurements of the mean flow and turbulence quantities including third-order moments are reported for all stations, documenting a well-established equilibrium flow even at higher-order moments. Sufficient information has been provided to compute the budgets for the turbulent

kinetic energy and the main shear stress, allowing the effects of adverse pressure gradients on the turbulent structure to be studied.

## 2. Experimental details

The experiment was performed in a closed return wind tunnel, fitted with an 11.5:1 contraction leading up to a 6 m long test section as shown in figure 1. The inlet cross-section was $1400 \times 280$ mm$^2$, giving an aspect ratio of 5:1. The investigated boundary layer developed on the flat floor, made of polished aluminium plates. The pressure gradient was generated by means of an adjustable roof. An initial estimate for the shape of the roof was obtained using a boundary-layer prediction code. From this geometry the final shape was iterated by a number of careful adjustments. After each adjustment a number of velocity profiles at different streamwise positions were measured using Pitot tubes to check if equilibrium had been established. The final height of the roof above the test surface (in mm) may be expressed as

$$h(x) = 280 - 49.9x - 47.69x^2 + 89.348x^3 - 31.358x^4 + 4.434x^5 - 0.2289x^6, \qquad (1)$$

where $x$ is measured in metres from the beginning of the test section. The free-stream turbulence level, $(\overline{u^2})^{\frac{1}{2}}/U_e$, at the first measurement station ($x = 3.0$ m) was less than 0.35%.

The wall static pressure distribution was measured using 66 wall taps, 1 mm in diameter, connected to two SETRA transducers by means of two Scanivalves. The first tap was located at $x = 0.1$ m and the following taps were located at 0.2 m intervals. At 1 m intervals 7 taps were distributed across the test section to allow the two-dimensionality of the flow to be checked. The two-dimensionality was also checked by measurements of the skin friction coefficient across the test section at a number of streamwise positions using Preston tubes. This showed that $C_f$ remained constant within $\Delta C_f = \pm 1.1 \times 10^{-5}$ across the entire span of the test section, corresponding to $\pm 18$% of the mean value in the equilibrium region. No indications of secondary flow type streamwise vortices were found to be present in the boundary layer. The two-dimensionality of the flow in the freestream was checked at a number of streamwise stations by measuring the flow angle in the plane parallel to the test surface by means of an X-wire traversed across the test section. This angle was found to be symmetric about the centreline and to vary linearly across the flow. The maximum value was found close to the edge of the sidewall boundary layers where its value agreed with the boundary-layer growth rate. The two-dimensionality was also checked by streamwise integration of the momentum equation using the boundary-layer parameters from the profiles measured along the centreline. The momentum balance was performed along the guide lines of Coles & Hirst (1968) and was found to be satisfied over the entire measurement domain to within 1.9% of $U_e^2\theta$ at the first measurement station ($x = 3.0$ m). Finally velocity profiles were measured at a number of stations off the centreline. No systematic spanwise variations were detected. From these checks it was concluded that the two-dimensionality of the flow was good.

A 2 mm trip wire, located at $x = 0.05$ m, was used to ensure that the boundary layer was turbulent. The boundary layer was allowed to develop under the influence of a slight favourable pressure gradient for 1 m before the adverse pressure gradient started. This was done to stabilize and mature the boundary layer over a short distance and to reduce the effect of the disturbances from the trip wire.

Velocities were measured by means of single hot wire and X-wire probes of different geometries, allowing measurements of $u$ and $v$, or $u$ and $w$, respectively. The wires were

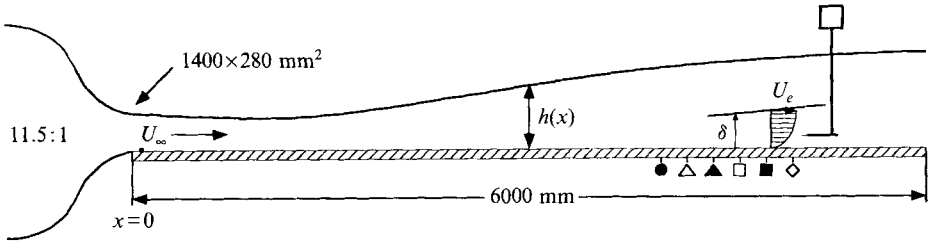


FIGURE 1. Wind-tunnel working section. The first measurement station is at $x = 3000$ mm and subsequent stations are located at 200 mm intervals. Symbols used for the stations presented are also shown.

made of 2.5 μm platinum – 10% rhodium Wollaston wire, etched to a nominal wire length of 0.5 mm, giving a length in wall units of about $l^+ \approx 11$. The wire separation was about $\Delta z^+ \approx 6.5$. The apex angles of the X-wire probes were kept close to 110°, since low velocities combined with high turbulence intensities, which would produce large instantaneous flow angles, were expected near the wall. (See Perry, Lim & Henbest 1987, and Krogstad, Antonia & Browne 1992, for further discussions about probe apex angle effects.) All wires were operated with in-house constant-temperature anemometers at an overheat ratio of 1.5. The hot-wire probes were calibrated in the tunnel free stream for velocity and angular sensitivity using the effective angle approach of Browne, Antonia & Chua (1989). The anemometer outputs, low-pass filtered at 10 kHz, were sampled at 20 kHz at 12 bit resolution to a Compaq 386 personal computer using a 16 channel A/D system from R C Electronics. The data were sampled for 21 s and transferred to a VAX 3100 cluster for post-processing.

## 3. Results and discussion

### 3.1. *Equilibrium flow*

It is generally accepted that the flows close to a solid surface exhibit similarity characteristics when scaled using inner variables, i.e. the friction velocity $u_\tau = (\tau_w/\rho)^{\frac{1}{2}}$ and the viscous lengthscale $\mu/\rho u_\tau$. This similarity manifests itself in the well-known viscous sublayer and the logarithmic law of the wall. In order to have similarity also in the outer flow, the streamwise momentum equation shows that equilibrium in the velocity defect function and the shear stress profile must be assumed. This may only be obtained if a number of restrictions on the development of the relevant length and velocity scales are satisfied (Townsend 1976). These are derived from the equations of momentum and turbulent kinetic energy. It is found that equilibrium can only exist if the free-stream velocity, $U_e$, varies as a power of the streamwise distance, i.e. $U_e \sim (x-x_0)^{-m}$, where $x_0$ is the virtual origin of the equilibrium state. The exponent $m$ is found to be in the region $0 < m < 0.23$ for non-separating adverse pressure gradient flows (Mellor & Gibson 1966). It also follows that the ratio of the thickness of the inner and outer layer must be constant and that all lengthscales must be linearly proportional to the same distance, i.e. $L \sim (x-x_0)$. This implies a constant shape factor $H = \delta^*/\theta$ where $\delta^*$ is the displacement thickness and $\theta$ the momentum thickness. Also the ratio between the shear and free-stream velocities, $u_\tau/U_e$, must remain constant. As a consequence the skin friction coefficient, $C_f$, and the non-dimensional pressure gradient, $\beta = (\delta^*/\tau_w)\,\mathrm{d}P/\mathrm{d}x$, become constants. When these requirements are fulfilled, the velocity defect profile and the Reynolds shear stress distribution should be self similar when scaled with the proper velocity variables. Still there is some disagreement

in the literature as to what the proper scaling is (see George & Castillo 1993; Perry, Marušic & Li 1993). It will be shown in the next section that in the present experiment $C_f$ is constant in the equilibrium region. The velocity defect profiles will therefore show similarity whether scaled in the conventional way as $(U_e - U)/u_\tau$, using $u_\tau$ as the proper velocity scale for the mean flow, or as $(U_e - U)/U_e$, as proposed by George & Castillo.

### 3.2. *Mean flow*

In the present experiment a low skin friction coefficient was aimed for. Therefore reversed flow events may occur close to the wall, possibly introducing severe errors in the velocity measurements. Separation was found to appear first in the boundary layer developing along the curved roof used to generate the pressure gradient. After establishing the equilibrium layer on the test floor, we made sure that all surfaces were free from separated regions by means of flow visualizations using tufts. In the equilibrium part of the flow $C_f$ was of the order of $6.0 \times 10^{-4}$ or about one fifth of the value expected for zero pressure gradient boundary layers. According to the pulsed hot-wire measurements of Dengel & Fernholz (1990), $C_f$ may be as low as $3.5 \times 10^{-4}$ before reversed flow is encountered. When inspecting the statistics of the velocity vector measured by the X-wire probes, no indications of unacceptably large flow angles were found. Nowhere were more than 0.4% of the measurements found to lie outside $\pm\frac{1}{4}$ of the apex angle, i.e. about $\pm 30°$. Thus the measurements are believed to be free from errors connected to excessive flow angles.

In order to quickly produce a flow with low skin friction, a strong adverse pressure gradient with $\mathrm{d}P/\mathrm{d}x > 0$ and $\mathrm{d}^2P/\mathrm{d}x^2 > 0$ was imposed on the flow, bringing it close to separation. To keep $C_f$ constant, the pressure gradient was then relaxed to the required shape ($\mathrm{d}P/\mathrm{d}x > 0$, $\mathrm{d}^2P/\mathrm{d}x^2 < 0$) producing a stable equilibrium boundary layer. The measurement stations were located at 0.2 m intervals for $3.0 \leqslant x \leqslant 5.2$ m. Equilibrium was established for $4.0 \leqslant x \leqslant 5.0$ m and only these profiles will be shown.

The friction velocity, $u_\tau$, was obtained in a number of independent ways. By applying a least-square fit of the law of the wall and a wake function to the measured mean velocity data, $u_\tau$ may be obtained. The Musker (1979) explicit function was used to represent the velocity profile. This function applies to both the viscous layer and the fully turbulent wall region, as well as the wake region in the outer part, where the Granville (1976) wake function is used. The direct numerical simulation (DNS) results of Spalart & Leonard (1987) and Spalart & Watmuff (1993) for turbulent boundary layers subjected to pressure gradients indicate that the law of the wall may be affected by the gradient. As the adverse pressure gradient increased, the level of the log law was found to shift down and the apparent value of the von Kármán constant, $\kappa_u$, decreased. However, the functional dependency is not known and it is also possible that a part of this shift may be a Reynolds-number effect, since increasing the Reynolds number has been found to produce similar effects in zero pressure gradient DNS (Spalart 1988). For the analysis of the present data, conventional values were therefore used ($\kappa_u = 0.41$ and $B = 5.2$).

The fit procedure contains three unknowns, $u_\tau$, $\Pi$ and $\delta$ which were obtained by iteration using a multi-variable optimization technique (Krogstad *et al.* 1992). (In this way the definition of the boundary-layer thickness is linked directly to the mathematical representation of the profile rather than to the imprecise definition of where the mean velocity reaches a certain fraction of the free-stream velocity, e.g. 99.5%. This produces values of $\delta$ which are very sensitive to experimental scatter.) Owing to the strong pressure gradient, the wake parameter, $\Pi$, grew to about 7. This is more than 10 times the value normally accepted for zero pressure gradient layers.

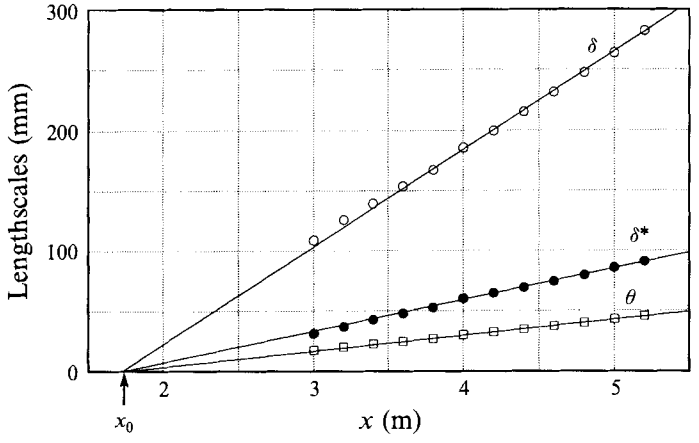


FIGURE 2. Development of boundary-layer thickness, $\delta$, displacement thickness, $\delta^*$, and momentum thickness, $\theta$.

| $x$ [m] | $h$ [mm] | Symbols used | $U_e$ [m s$^{-1}$] | $\delta$ [mm] | $\theta$ [mm] | $H$ [−] | $G$ [−] | $\beta$ [−] | $C_f \times 10^3$ [−] | $Re_\theta$ [−] | $\Pi$ [−] |
|---|---|---|---|---|---|---|---|---|---|---|---|
| 3.0 | 484 | — | 22.35 | 109.0 | 17.56 | 1.793 | 20.8 | 12.2 | 0.900 | 25400 | 4.60 |
| 3.2 | 513 | — | 21.92 | 125.7 | 20.14 | 1.840 | 22.9 | 14.0 | 0.797 | 28420 | 5.20 |
| 3.4 | 541 | — | 21.21 | 139.4 | 22.60 | 1.901 | 24.8 | 15.7 | 0.730 | 30910 | 5.65 |
| 3.6 | 567 | — | 20.53 | 153.8 | 24.84 | 1.936 | 26.4 | 16.9 | 0.672 | 33020 | 6.00 |
| 3.8 | 591 | — | 20.10 | 167.2 | 27.03 | 1.957 | 27.0 | 17.3 | 0.654 | 34570 | 6.16 |
| 4.0 | 610 | ● | 19.81 | 185.6 | 30.13 | 2.006 | 29.2 | 19.9 | 0.590 | 39120 | 6.75 |
| 4.2 | 630 | △ | 19.42 | 199.7 | 32.54 | 1.999 | 29.3 | 20.0 | 0.582 | 41580 | 6.80 |
| 4.4 | 647 | ▲ | 19.38 | 215.3 | 34.83 | 1.989 | 29.1 | 19.6 | 0.585 | 44420 | 6.75 |
| 4.6 | 662 | □ | 18.84 | 231.7 | 37.35 | 1.998 | 29.6 | 20.1 | 0.571 | 46250 | 6.85 |
| 4.8 | 676 | ■ | 18.67 | 247.4 | 39.98 | 1.994 | 29.6 | 20.2 | 0.567 | 49180 | 6.90 |
| 5.0 | 687 | ◇ | 18.30 | 263.7 | 42.98 | 1.998 | 30.2 | 21.2 | 0.546 | 50980 | 7.10 |
| 5.2 | 700 | — | 18.04 | 282.9 | 45.78 | 1.986 | 30.2 | 21.4 | 0.541 | 53970 | 7.15 |

TABLE 1. Characteristic boundary-layer parameters in the region $3.0 \leqslant x \leqslant 5.2$ m.

To confirm the $C_f$ found from the best fit procedure, Preston tubes of 1.0, 3.0 and 9.0 mm outer diameter were also used, all producing the same values for $C_f$. The skin friction coefficient was obtained using the calibration curves of Patel (1965) and all measurements were taken for conditions well within the 6% maximum error limits specified for adverse pressure gradients. The $C_f$ values obtained from the Preston tubes were consistently found to be slightly higher than the values obtained from the fit. This could be due to the high turbulence level found near the wall in this flow. The measured pressure signal is contaminated by the turbulent normal stresses causing the reading to be too high, which in turn exaggerates $C_f$. The largest difference between $C_f$ from the mean velocity fit and the Preston tube reading was only of the order of 10%, found in the equilibrium region where $C_f$ was at its lowest. However, the results from the two methods follow each other closely in the whole measurement domain as may be seen from figure 4(*a*). It should be mentioned that if the log law is shifted down by the pressure gradient, as suggested by the DNS results, a higher $C_f$ would be obtained from the fit, improving the agreement between the two methods.

The experimental conditions are listed in table 1. These are the height of the tunnel at the measurement stations, as well as the distributions of the free-stream velocity, the

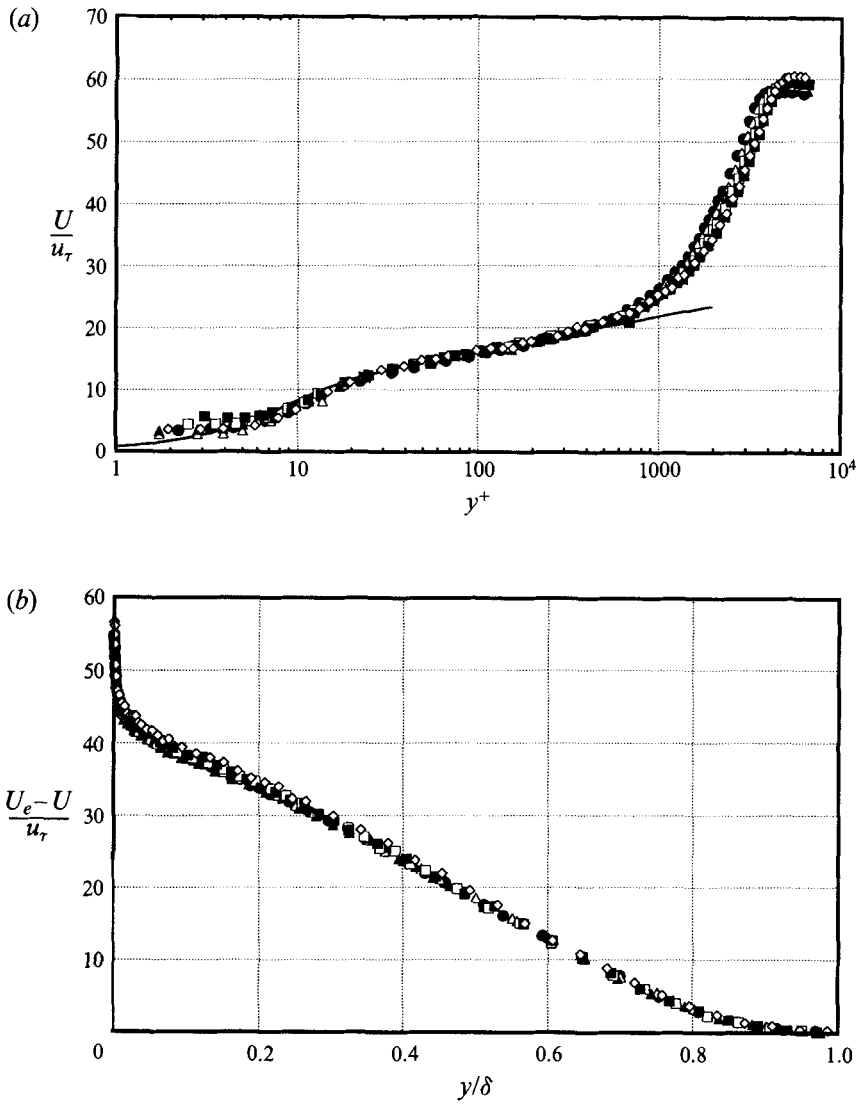


FIGURE 3. (*a*) Streamwise mean velocity plotted in wall variables. Symbols are defined in table 1. ——, $U/u_\tau = 2.44\ln(y^+)+5.2$. (*b*) Velocity defect profiles.

boundary-layer and momentum thicknesses, the shape factor, the Clauser parameter, $G = (H-1)/(H(\frac{1}{2}C_f)^{\frac{1}{2}})$, the non-dimensional pressure gradient, the skin friction coefficient from the mean velocity profile, the Reynolds number based on the momentum thickness, $Re_\theta$ and the wake strength, $\Pi$. Also given are the symbols used in the successive plots. At these stations equilibrium is assumed to exist.

Figure 2 shows that the lengthscales such as $\delta$, $\delta^*$ and $\theta$ grow linearly with the streamwise distance for $x > 4.0$ m, as required for equilibrium boundary layers. In the equilibrium part the lengthscales have a common origin at $x_0 = 1.74$ m. Using this origin the free-stream velocity distribution was fitted to the equilibrium relation $U_e = U_{ref}(x-x_0)^{-m}$ giving $U_{ref} = 23.6$ m s$^{-1}$ and $m = 0.22$.

Equilibrium implies that the velocity profiles at all stations must be similar in the inner layer when scaled on inner variables, and in the outer layer when scaled on outer

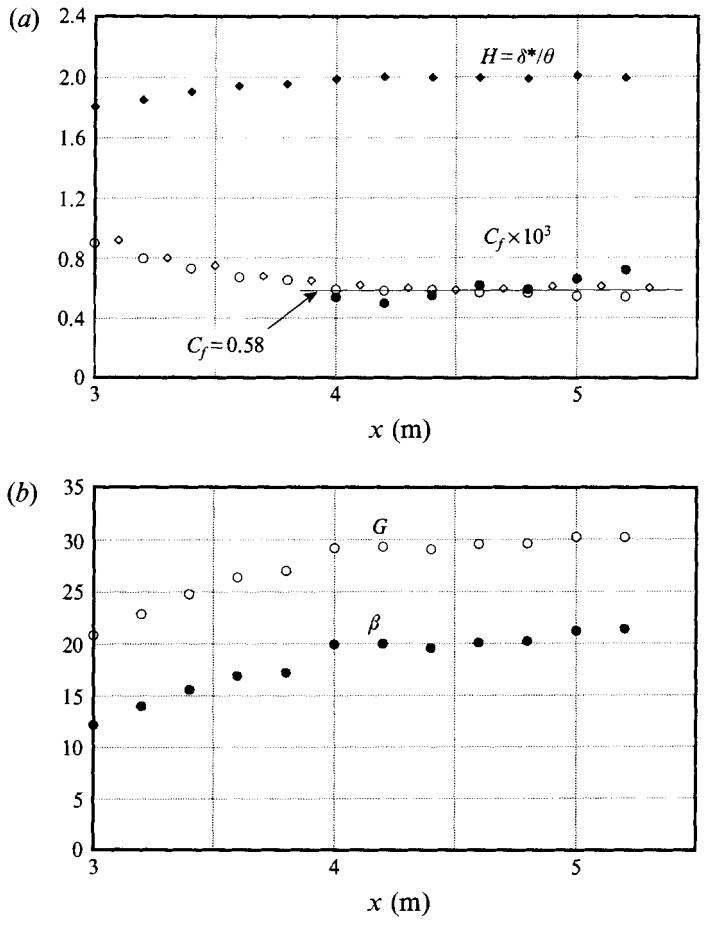


FIGURE 4. (*a*) Streamwise distributions of skin friction coefficient, $C_f$, and shape factor, $H$. ○, best fit to mean velocity profiles; ◇, Preston tubes; ●, from $-\overline{uv}$ profiles. (*b*) Streamwise distributions of ○, the Clauser factor $G$ and ●, the pressure gradient parameter $\beta$.

variables. Figure 3(*a*) documents the inner-layer similarity and shows that the wake is a very dominant part of this flow. (No corrections for wall effects were applied to the data. These effects are normally assumed to affect the measurements for $y^+ \leqslant 5$ and explain the scatter in this region. Correction methods (e.g. Oka & Kostic 1972) exist which force the data to follow the distribution $U^+ = y^+$ close to the wall. Since these corrections cannot be considered to be better than curve fits they were not applied. In the present flow the viscous sublayer is very thin compared to the boundary-layer thickness and the main interest of the present paper lies in the outer-layer similarity, so the scatter was not considered to be serious.) The velocity defect (figure 3*b*) shows that outer-layer similarity has also been obtained. The velocity profile similarity is also documented in the table, since the skin friction coefficient, the shape factor and the Clauser parameter remain constant at about $5.7 \times 10^{-4}$, 2.0 and 29.3 respectively in the equilibrium region. These parameters have been shown in figure 4 which documents that equilibrium was established for $x > 4.0$ m. The skin friction coefficient from the Preston tube in this region was about $6.0 \times 10^{-4}$.

The Clauser parameter $G$ plotted against $\beta$ is shown in figure 5. Results from some

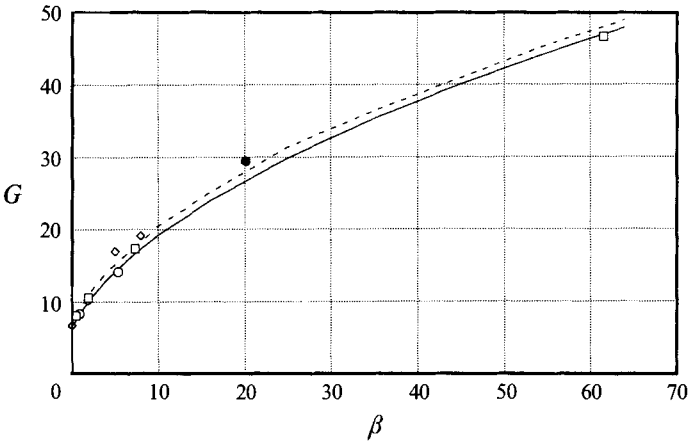


FIGURE 5. Correlation between the Clauser factor $G$ and the pressure gradient parameter $\beta$ for equilibrium flows. ◇, Clauser 1954; ○, Bradshaw 1967; □, East & Sawyer 1979; ●, present; ——, Nash 1965; -----, Mellor & Gibson 1966.

previously reported equilibrium boundary-layer experiments have been included for comparison. The present data are seen to follow the trend of the other data well and agree with the relations proposed by Nash (1965) and Mellor & Gibson (1966).

### 3.3. *Turbulent stresses*

All normal stresses, $\rho\overline{u^2}$, $\rho\overline{v^2}$, $\rho\overline{w^2}$, as well as the shear stresses $-\rho\overline{uv}$ and $-\rho\overline{uw}$ were measured. It was shown by Krogstad & Skåre (1993) that by scaling the turbulent shear stresses with the value of $u_\tau$ obtained from the best-fit procedure, similarity in the turbulent stresses was not obtained to the same degree as for the mean velocity. As commented earlier there may be some uncertainty in deriving $u_\tau$ this way if the exact level of the logarithmic layer is not known. Using the measured mean velocity profiles, the corresponding shear stress distribution may be computed from the streamwise momentum equation. Comparing this with the measured profile, another estimate for $u_\tau$ may be derived. Procedures have been devised for zero pressure gradient flows (e.g. Granville 1988; Li & Perry 1989). Here the method of Granville was extended to include the adverse pressure gradient and the gradients of the normal stresses $(\partial/\partial x)(\overline{u^2}-\overline{v^2})$. Although these stresses become more important as the pressure gradient increases, their contribution to the computed shear stress profile was only of the order of 3% of the peak value. As for the fit procedure, the mean velocity profile was again described using the Musker formulation. Inserted in the momentum equation and assuming equilibrium flow, a differential equation for the total shear stress gradient is derived which was integrated numerically. This equation contains $U_e$, $\Pi$, $\delta$ and $C_f$ as well as the gradients $\mathrm{d}U_e/\mathrm{d}x$ and $\mathrm{d}\delta/\mathrm{d}x$ as parameters. These were well known from the mean velocity measurements and were applied as measured. The equation for the shear stress gradient is a first-order equation which only satisfies one boundary condition, taken to be $\tau = \tau_w$ at the wall. Using the measured values for $U_e$, $\Pi$ etc. there is no guarantee that the computed distribution goes exactly to zero at the boundary-layer edge. To satisfy this condition as well, it was found necessary to decrease $\mathrm{d}\delta/\mathrm{d}x$ by 3% compared to the measured value. Another estimate for $C_f$ could then be obtained from the measured shear stresses by adjusting $u_\tau$ used to scale the data until the measured profile agreed with the calculations.

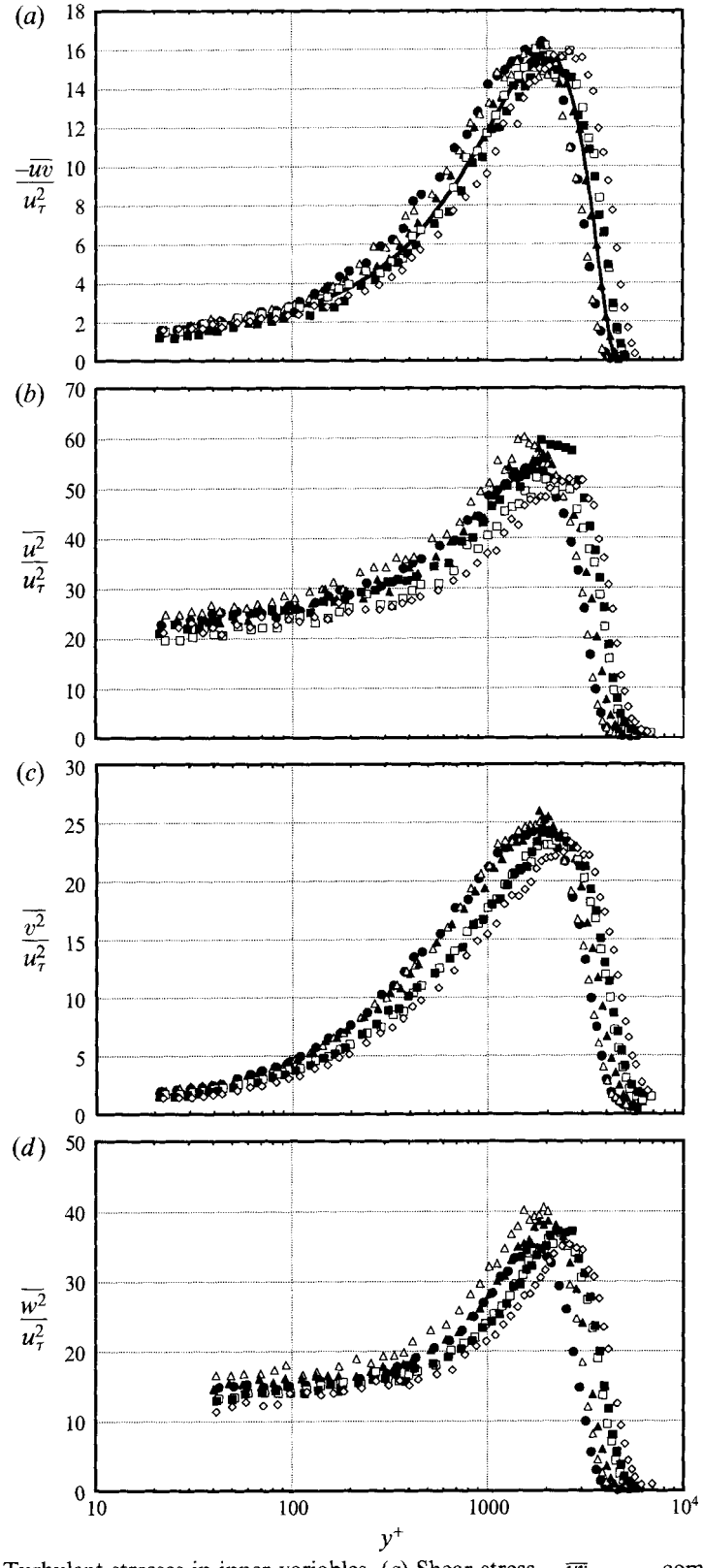


FIGURE 6. Turbulent stresses in inner variables. (*a*) Shear stress $-\overline{uv}$. ——, computed from velocity profile at $x = 4.4$ m. Normal stresses: (*b*) $\overline{u^2}$, (*c*) $\overline{v^2}$, (*d*) $\overline{w^2}$.

These estimates for $C_f$ are also shown in figure 4(*a*) and the agreement with the Preston tubes and the profile fits is seen to be good, considering the higher uncertainties involved in the measurements of shear stress. $C_f$ from the shear stress profiles increases slightly downstream, while the estimates from the mean velocity profiles decrease slightly and the Preston tube data are virtually independent of $x$. The slight disagreement between the different methods is assumed to be due to experimental scatter, but could also indicate that the boundary layer has only reached approximate equilibrium. However, it should be pointed out that when the gradient in $C_f$ from the shear stress profiles was included in the computations for the shear stress profile, unacceptable results were produced. At $y = \delta$ the calculated stress was still as high as $\tau^+ \approx 5$ and could only be brought back to zero by making severe changes to the other parameters away from their measured values. Hence the small skin friction gradient appears to be incompatible with the mean velocity profiles and is therefore assumed to be due to experimental scatter. Using $C_f$ from the shear stress profiles to normalize $-\overline{uv}$, the profiles are seen to collapse well. The distribution obtained from the calculations is also included and the measurements are seen to follow this line closely.

The turbulent stresses scaled in inner variables are presented in figure 6 and in outer variables in figure 7. Equilibrium is seen to exist for all stresses both in the inner and outer layer, although the scatter in $\rho\overline{u^2}$ and $\rho\overline{w^2}$ is somewhat high. The Reynolds number increases by almost 50% from the first to the last station of the equilibrium region. As expected this is seen to produce a shift in the stress profiles towards higher $y^+$ in the outer layer when scaled in inner variables. Owing to the strong pressure gradient, the dominant Reynolds shear stress $-\rho\overline{uv}$ reaches values which are considerably higher than the wall shear stress, $\tau_w$. The maximum value is located roughly midway through the layer ($y/\delta \approx 0.45$) as shown in figure 7(*a*). The peak in the present experiment was $-\rho\overline{uv}_{max}/\tau_w \approx 15.7$. This level must depend on the non-dimensional pressure gradient, since $\beta$ determines the gradient of the stress profile at the wall. (In the immediate vicinity of the wall the shear stress distribution may be written $(\tau/\tau_w) = 1 + (y/\tau_w)(\mathrm{d}p/\mathrm{d}x) = 1 + (y/\delta^*)\beta$.) Figure 8 shows that $-\rho\overline{uv}_{max}/\tau_w$ scales linearly with $\beta$, closely following the line $-\rho\overline{uv}_{max}/\tau_w = 1 + \frac{3}{4}\beta$. The peak found in the present experiment agrees well with the findings of Bradshaw (1967) and East & Sawyer (1979).

It may be argued that since the ratio between the maximum shear stress, $-\overline{uv}_{max}$, and $u_\tau^2$ is very large, $u_\tau$ may no longer be the relevant parameter for scaling the turbulent stresses in the outer region and that scaling with $-\overline{uv}_{max}$ would be preferable. However, owing to the similarity of the stresses it follows that other ways of scaling, such as $\overline{uv}/\overline{uv}_{max}$ *vs.* $y/\delta$ or $(\overline{uv}_{max} - \overline{uv})/\overline{uv}_{max}$ *vs.* $y/\delta$ will exhibit the same degree of similarity. Therefore there seems to be no benefit in departing from the conventional use of $u_\tau$ as the scaling velocity for the turbulent stresses in this case.

As discussed in §3.1 and shown by the computed shear profiles, equilibrium in the mean flow is closely linked to similarity in the Reynolds shear stresses. Based on the same type of arguments, similarity would therefore also be expected in the normal stress profiles if the shear stresses show similarity. The normal stresses are shown in figures 6(*b–d*) and 7(*b–d*) which document the stresses to be similar, both plotted in inner and outer variables. Close to the wall $\overline{w^2}$ closely follows the development of $\overline{u^2}$. For the intermediate range $0.03 < y/\delta < 0.15$ the growth rate of $\overline{w^2}$ is somewhat slower than for $\overline{u^2}$, before they again increase at about the same rate. It appears that in this intermediate range the growth of $\overline{v^2}$ is favoured to the detriment of $\overline{w^2}$. A possible explanation for this behaviour is offered in §4.2, where skewness and flatness distributions are discussed.

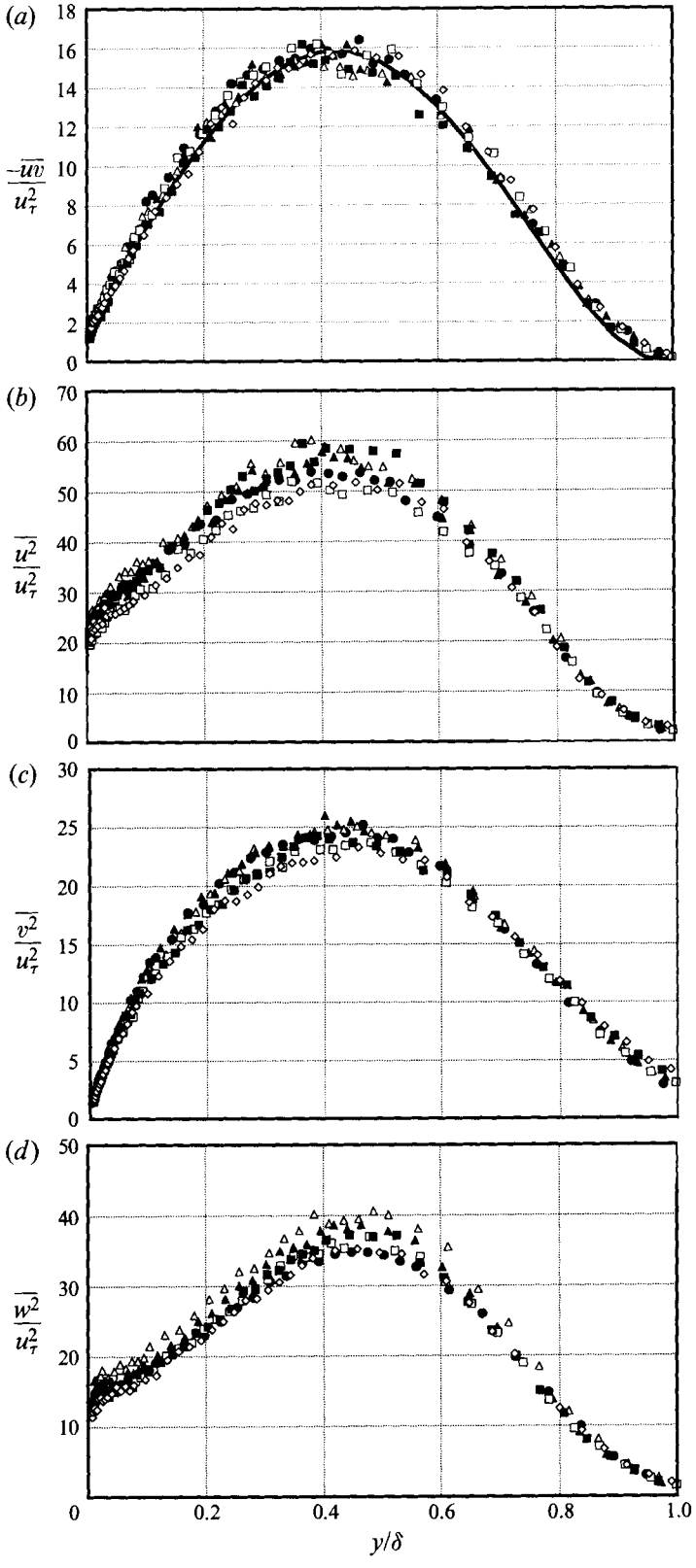


FIGURE 7. Turbulent stresses in outer variables. (*a*) Shear stress $-\overline{uv}$. ——, computed from velocity profile at $x = 4.4$ m. Normal stresses: (*b*) $\overline{u^2}$, (*c*) $\overline{v^2}$, (*d*) $\overline{w^2}$.

All normal stresses and the kinetic energy reach their peak values at the same location from the wall. By inspecting the transport equation for the turbulent stress $\overline{u_i u_j}$,

$$U_k \frac{\partial \overline{u_i u_j}}{\partial x_k} = -\overline{u_j u_k}\frac{\partial U_i}{\partial x_k} - \overline{u_i u_k}\frac{\partial U_j}{\partial x_k} - \frac{\partial \overline{u_i u_j u_k}}{\partial x_k} - \frac{1}{\rho}\left(\frac{\partial \overline{p u_j}}{\partial x_i} + \frac{\partial \overline{p u_i}}{\partial x_j}\right) + \frac{1}{\rho}\overline{p\left(\frac{\partial u_j}{\partial x_i} + \frac{\partial u_i}{\partial x_j}\right)} + \frac{\mu}{\rho}\frac{\partial^2 \overline{u_i u_j}}{\partial x_l \partial x_l} - \frac{2\mu}{\rho}\overline{\frac{\partial u_i}{\partial x_l}\frac{\partial u_j}{\partial x_l}}, \quad (2)$$

it is found that the dominant turbulence production terms for a two-dimensional boundary layer are $-\overline{uv}\,\partial U/\partial y$, which occur in the equation for $\overline{u^2}$, and $\overline{v^2}\,\partial U/\partial y$, which is found in the equation for $-\overline{uv}$. These terms have been plotted in figure 9. It may be observed that both terms exhibit two distinct peaks, one near the wall and another further out at $y/\delta \approx 0.45$. The exact location of the innermost peak could not be found, since the size limitations of the X-wire prevented measurements closer to the wall than about $y^+ \approx 20-30$, but it appears reasonable to assume that it will be found at about $y^+ \approx 12$ as observed in the zero pressure gradient case (Spalart 1988). The peak near the wall is caused by the increasing mean strain as the wall is approached so that the production increases until $-\overline{uv}$ diminishes near the wall. The outer peak, however, is caused by the peak in the turbulent stresses and is therefore linked directly to the effect of the strong adverse pressure gradient.

### 3.4. *Mixing length*

The mixing lengths derived from the mean velocity and $-\overline{uv}$ profiles are shown in figure 10. The slope of the mixing length near the wall, $\kappa_l$, is about 0.41 at the beginning of the logarithmic layer. This is the value normally accepted for zero pressure gradient flows. However, $\kappa_l$ is seen to increase rapidly through the logarithmic layer to a value of $\kappa_l \approx 0.78$. This indicates a very strong dependence of $\kappa_l$ on the pressure gradient. Further out ($0.15 < y/\delta < 0.9$) the value of $l/\delta$ remains roughly constant at 0.07 to 0.08, slightly below the zero pressure gradient boundary-layer value. Granville (1989) gives a review of how the effect of pressure gradients on the mixing length is modelled in the inner layer and proposes the model,

$$\frac{l}{\delta} = \kappa_l \frac{y}{\delta}(1+\alpha P^+ y^+)^{\frac{1}{2}}(1-\exp(-y^+(1+14P^+)^{\frac{1}{2}}/26)), \quad (3)$$

for adverse pressure gradients. Here

$$P^+ = \frac{\mu}{\rho^2 u_\tau^3}\frac{\mathrm{d}P}{\mathrm{d}x} = \frac{\mu\beta}{\rho u_\tau \delta^*}.$$

This expression is readily derived from the momentum equation except for the exponential function which represents a van Driest type damping. $\alpha$ was specified as being less than 1 to produce a reduction in the effective pressure gradient due to the mean flow inertia. This reduction was estimated by Perry, Bell & Joubert (1966) to be approximately one-third giving $\alpha = \frac{2}{3}$, while Granville specified $\alpha = 0.9$. Equation (3) is included in figure 10(*a*) and is seen to predict the mixing length well up to $y^+ \approx 250$. (The value for $\alpha$ specified by Granville was used since this represented the data slightly better than the value given by Perry *et al.*)

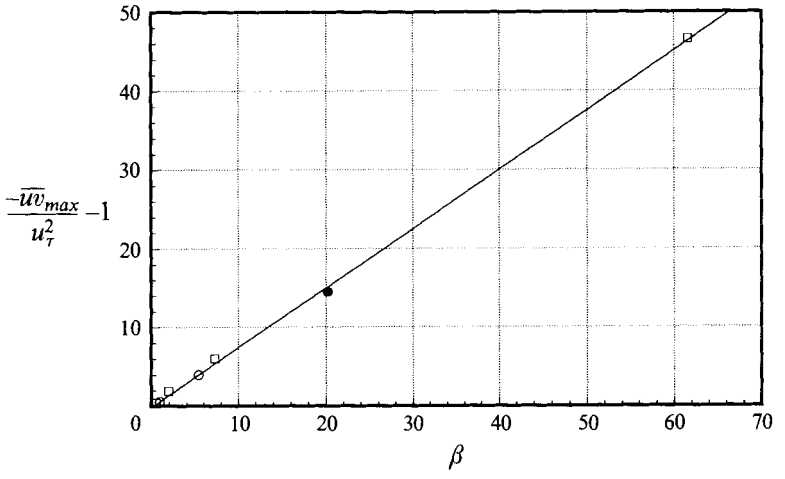


FIGURE 8. Maximum shear stress as function of $\beta$. Symbols as in figure 5.

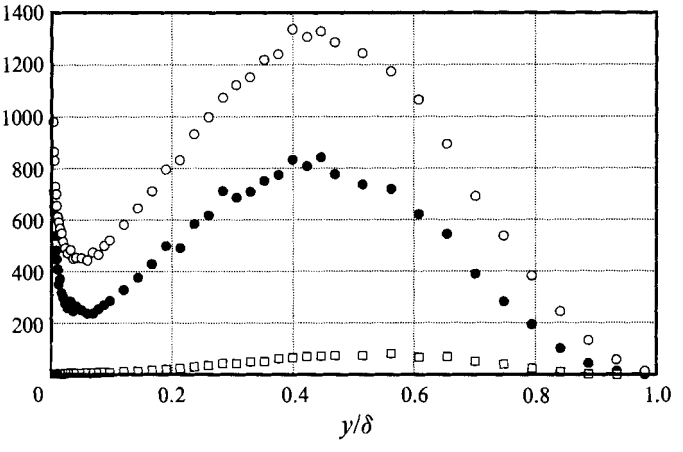


FIGURE 9. Contributions to turbulent production at $x = 4.4$ m.

$\bigcirc$, $\overline{v^2}\frac{\partial U}{\partial y}\frac{\delta}{u_\tau^3}$; $\bullet$, $-\overline{uv}\frac{\partial U}{\partial y}\frac{\delta}{u_\tau^3}$; $\square$, $(\overline{v^2}-\overline{u^2})\frac{\partial U}{\partial x}\frac{\delta}{u_\tau^3}$.

Despite the high $\kappa_l$ derived from the shear stress profile, the von Kármán constant in the logarithmic part of the mean flow, $\kappa_u$, was found to be the same as in the zero pressure gradient case. This confirms the findings of Perry *et al.* that 'the pressure gradient does not distort the logarithmic profile but simply controls its range of application of $y$ for a given wall shear velocity'. However, this does not comply with the DNS results.

Glowacki & Chi (1972) investigated equilibrium flows at different values of $\beta$. They found that the average $\kappa_l$ in the inner layer correlated well with $\beta$ in such a way that $\kappa_l$ increases rapidly with $\beta$ as shown in figure 11. The present results support this dependency. For flows where $\beta$ is changing in the streamwise direction, $\kappa_l$ is dependent on the flow development and cannot be correlated directly to the local $\beta$. For calculations using the mixing-length hypothesis, a rate of change equation for $\kappa_l$ would

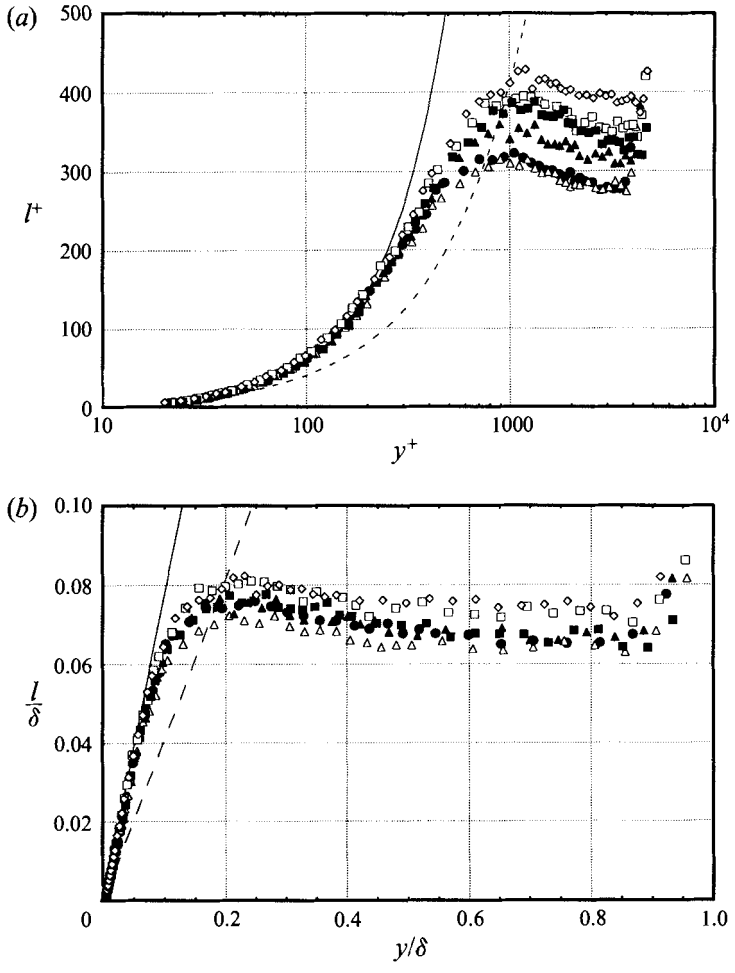


FIGURE 10. Mixing-length profiles. (*a*) Inner scaling: -----, $l^+ = 0.41y^+$; ——, Granville 1989. (*b*) Outer scaling: -----, $l/\delta = 0.41y/\delta$; ——, $l/\delta = 0.78y/\delta$.

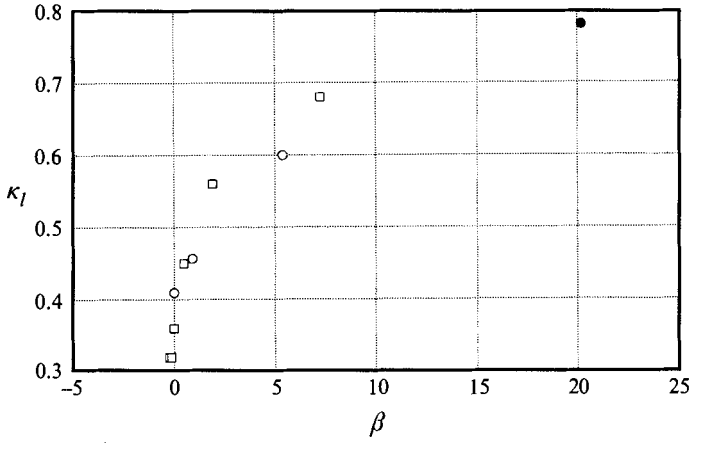


FIGURE 11. Dependence of $\kappa_l$ on $\beta$ in equilibrium boundary layers. For symbols see figure 5.

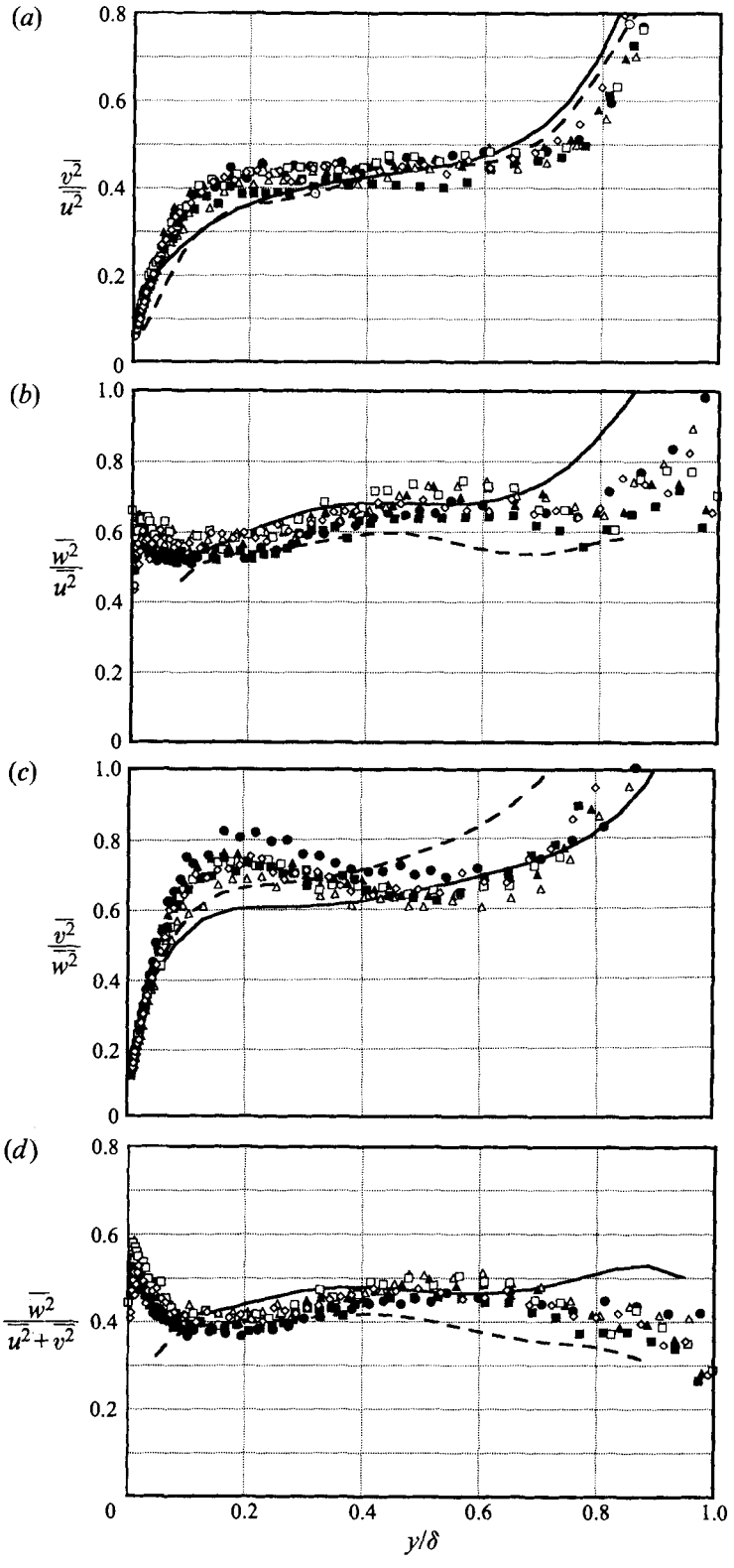


FIGURE 12(*a–d*). For caption see facing page.

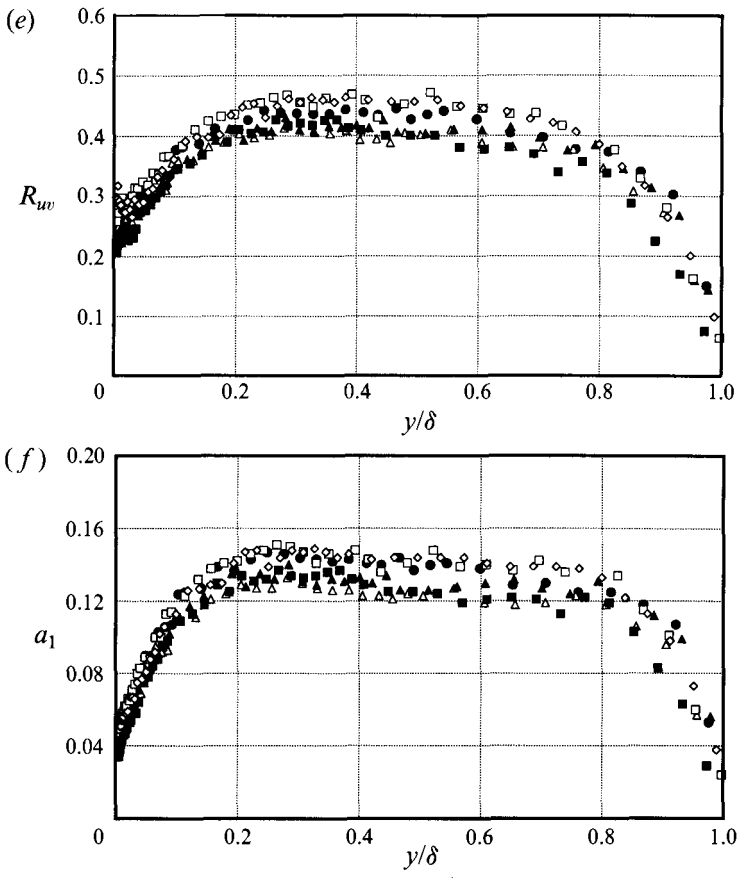


FIGURE 12. Second-order correlation ratios: (*a*) $\overline{v^2}/\overline{u^2}$, (*b*) $\overline{w^2}/\overline{u^2}$, (*c*) $\overline{v^2}/\overline{w^2}$, (*d*) $\overline{w^2}/(\overline{u^2}+\overline{v^2})$, (*e*) $R_{uv}$, (*f*) $a_1$. ——, Klebanoff ($Re_\theta \approx 8000$); -----, Spalart ($Re_\theta = 1410$).

therefore be necessary in order to predict $-\overline{uv}$ properly. However, since the slope of the logarithmic layer in the mean flow follows directly from the mixing-length formulation, it is difficult to see that a simple mixing-length hypothesis can successfully predict these observations.

### 3.5. *Turbulent correlation coefficients*

The ratios between the different Reynolds normal stresses, shown figure 12(*a–f*), show similarity for all stations. Also included are the zero pressure gradient data of Klebanoff (1955) at $Re_\theta \approx 8000$ and the DNS results of Spalart (1988) for $Re_\theta = 1410$. The agreement between the present set of measurements for strong adverse pressure gradients and the DNS data is about as close as between the two zero pressure gradient sets. This shows that the mechanism for redistributing the turbulent energy between the different normal stresses is virtually independent of the mean flow pressure gradient. As expected $\overline{v^2}$ is seen to vanish faster than $\overline{u^2}$ and $\overline{w^2}$ near the wall (figure 12(*a* and *c*)) owing to the stronger damping of fluctuations normal to the wall than in the planes parallel to it. For the main part of the boundary layer $\overline{v^2}/\overline{u^2}$ is roughly constant at about 0.45 while $\overline{w^2}/\overline{u^2}$ and $\overline{v^2}/\overline{w^2}$ are about 0.6 and 0.7, respectively. Near the boundary-layer edge, the ratios grow, primarily because $\overline{v^2}$ decays at a slower rate than $\overline{u^2}$ and $\overline{w^2}$. Therefore the ratio $\overline{w^2}/\overline{u^2}$ is virtually independent of $y/\delta$. Shiloh,

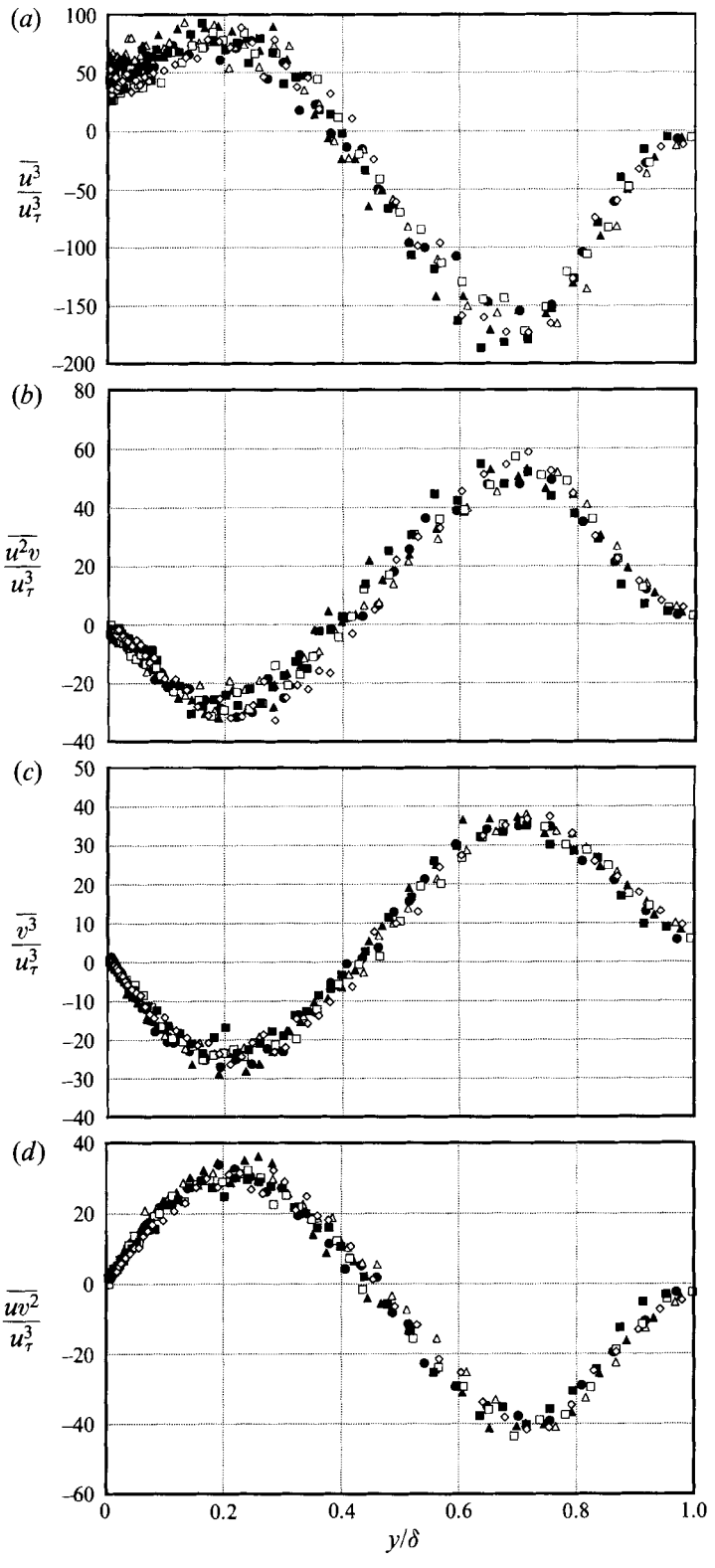


FIGURE 13(*a–d*). For caption see facing page.

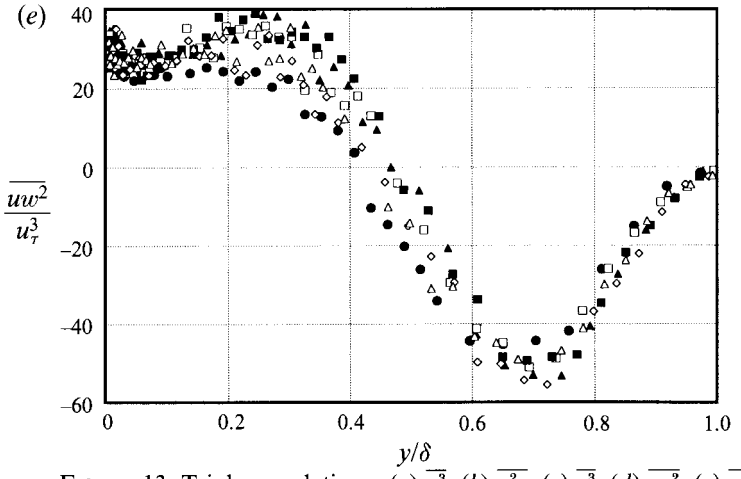


FIGURE 13. Triple correlations: (*a*) $\overline{u^3}$, (*b*) $\overline{u^2v}$, (*c*) $\overline{v^3}$, (*d*) $\overline{uv^2}$, (*e*) $\overline{uw^2}$.

Shivaprasad & Simpson (1981) proposed that $\overline{w^2}$ and $\overline{v^2}$ are approximately equal in the outer 90% of the boundary layer in flows near separation. The present experiment verifies that the ratio does not vary dramatically, although the factor is considerably lower than 1 (figure 12*c*).

When the spanwise normal stress $\overline{w^2}$ is not measured, it has often been assumed, e.g. in order to estimate the turbulent kinetic energy, that this stress may be linked to the other two through the relation $\overline{w^2} = K(\overline{u^2}+\overline{v^2})$, where $K = 0.5$ (Bradshaw 1967; Cutler & Johnston 1989). This expression seems to overestimate $\overline{w^2}$ slightly in most of the layer. Both the DNS and the present data indicate that $K \approx 0.4$ should be a better value, although figure 12(*d*) shows that the factor $K$ depends strongly on $y/\delta$ close to the wall.

Figure 12(*e*) shows the distribution of the correlation coefficient $R_{uv} = -\overline{uv}/(\overline{u^2})^{\frac{1}{2}}(\overline{v^2})^{\frac{1}{2}}$. $R_{uv}$ reaches a constant value for $0.2 < y/\delta < 0.7$. Although the figure indicates that this level varies between about 0.39 and 0.46, no systematic $x$-dependence in the data could be found. It is therefore assumed that the scatter in the data represents measurement uncertainty rather than any physical effects. Hence its value may be assumed to be about 0.42 for most of the layer, in close agreement with the value found in boundary layers without pressure gradients. Figure 12(*f*) shows the structure parameter $a_1 = -\overline{uv}/2k$, normally taken as 0.15 in zero pressure gradient flows. ($k = \frac{1}{2}(\overline{u^2}+\overline{v^2}+\overline{w^2})$ is the turbulent kinetic energy). In the present experiment it was found to be only slightly lower.

## 4. Higher-order statistics

### 4.1. *Triple correlations*

Seven of the nine triple correlations which may be formed from the fluctuating velocities, i.e. $\overline{u^3}$, $\overline{u^2v}$, $\overline{uv^2}$, $\overline{v^3}$, $\overline{u^2w}$, $\overline{w^3}$ and $\overline{uw^2}$, were measured. These quantities are associated with the transfer and redistribution of turbulent energy in the boundary layer. The four quantities measured by an X-wire in the $(x, y)$-plane, are $\overline{u^3}$, $\overline{u^2v}$, $\overline{v^3}$ and $\overline{uv^2}$. The largest term is the first correlation (figure 13*a*) which represents the transport of $\overline{u^2}$ by turbulent motion in the streamwise direction. Its magnitude is more than 3 times that of the other triple correlations. The next three correspond to the turbulent transport of $\overline{u^2}$ and $\overline{v^2}$ in the direction normal to the wall, and the turbulent work done

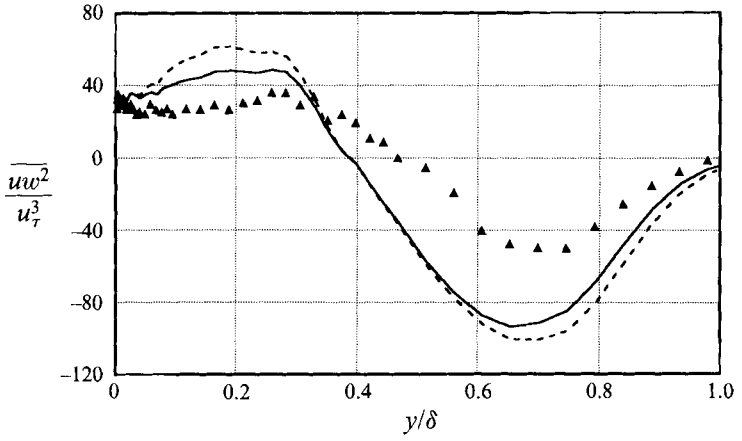


FIGURE 14. Estimated and measured $\overline{uw^2}$, shown for $x = 4.4$ m. ------, $K = 0.5$; ——, $K = f_{ww}(y/\delta)$ computed from figure 12(*d*).

by $-\overline{uv}$ in the same direction. These have been shown in figures 13(*b*)–13(*d*), respectively. For the turbulent transport normal to the wall, $\overline{u^2v}$ and $\overline{v^3}$ have opposite sign to $\overline{uv^2}$. Below the peak in turbulence production at $y/\delta \approx 0.45$ there is a downward transport of energy from $\overline{u^2}$, $\overline{v^2}$ and $-\overline{uv}$, while further out the diffusion is directed towards the edge of the layer. Figure 13 shows that similarity in the triple products has also been achieved.

Turbulent transport of $\overline{u^2}$ and $\overline{w^2}$ in the spanwise direction is expressed by $\overline{u^2w}$ and $\overline{w^3}$, while the transport of $\overline{w^2}$ in the streamwise direction is given by $\overline{uw^2}$. These terms were measured with an X-wire in the $(x, z)$-plane. The first two terms (not shown) which should vanish in a two-dimensional boundary layer were found to be very small. This supports further that the flow established is closely two-dimensional. The last term, plotted in figure 13(*e*), is showing a very slow decay below $y/\delta < 0.3$, while it follows the trend of the other correlations in the outer part of the boundary layer. This behaviour is similar to the development of $\overline{u^3}$ and suggests that close to the wall the transport of $\overline{w^2}$ is more efficient in the streamwise direction than normal to the wall. The correlations between the $v$ and $w$ fluctuations could not be measured with the present equipment. It may be observed that all the triple correlations show similar dependence of $y/\delta$, crossing zero where the maximum stresses occur. The maximum value of the triple correlations is for all variables found in the outer part of the boundary layer at $y/\delta \approx 0.75$. Another maximum, of opposite sign and with a smaller magnitude, is found in the inner part near $y/\delta \approx 0.25$. This is in contrast to the observations of Nagano, Tagawa & Tsuji (1991) in adverse pressure gradient flows at much lower Reynolds numbers ($Re_\theta \leqslant 3350$), where the inner peak was found to be the largest. However, the pressure gradient in the present case is considerably stronger which, as shown, increases the turbulent activity in the outer part of the boundary layer.

The same type of estimate which was used for $\overline{w^2}$ is also used to evaluate $\overline{uw^2}$, i.e. $\overline{uw^2} = K(\overline{u^3} + \overline{uv^2})$, where $K$ is again assumed to be 0.5 (e.g. Bradshaw 1967; Cutler & Johnston 1989). This seems to overestimate $\overline{uw^2}$ by a factor of two compared to the experimental data, as shown in figure 14. Another possibility is to use the correlation already obtained in figure 12(*d*) between $\overline{w^2}$ and $\overline{u^2} + \overline{v^2}$, i.e. defining $K = f_{ww}(y/\delta) = \overline{w^2}/(\overline{u^2} + \overline{v^2})$. As shown in figure 14 this gives an improvement close to the wall, but in the outer part $\overline{uw^2}$ is still considerably overestimated. The reason for this is that $\overline{uv^2}$ and

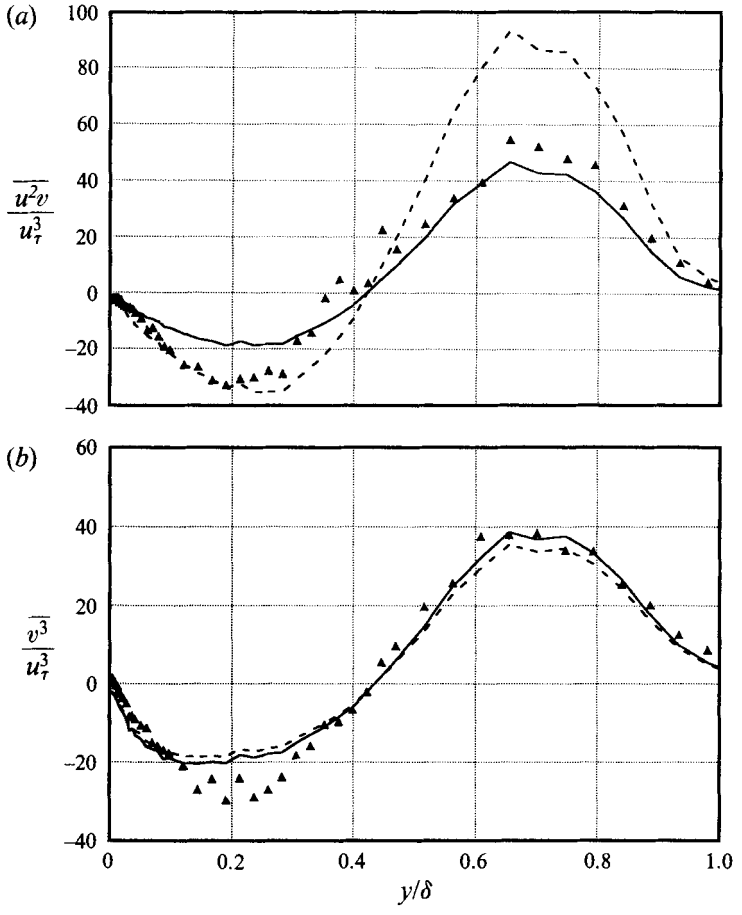


FIGURE 15. Triple correlations from the gradient diffusion hypothesis ($x = 4.4$ m). ——, equation (4); -----, equation (5); (*a*) $\overline{u^2v}$, (*b*) $\overline{v^3}$.

$\overline{uw^2}$ are roughly equal, while $\overline{u^3}$ is considerably larger (figure 13) and therefore dominates the estimate. Except very close to the wall ($y/\delta < 0.1$) a better estimate would be $\overline{uw^2} \approx \overline{uv^2}$.

In turbulence modelling triple correlations are frequently estimated from the Reynolds stresses using a gradient diffusion hypothesis. Hanjalic & Launder (1972) derived the relation

$$\overline{u_i u_j u_k} = -c_s \frac{k}{\epsilon}\left\{\overline{u_i u_l}\frac{\partial \overline{u_j u_k}}{\partial x_l} + \overline{u_k u_l}\frac{\partial \overline{u_i u_k}}{\partial x_l} + \overline{u_k u_l}\frac{\partial \overline{u_i u_j}}{\partial x_l}\right\}, \tag{4}$$

where $c_s = 0.08$. This relation is often simplified to

$$\overline{u_k u_i u_j} = -c_s \frac{k}{\epsilon}\overline{u_k u_l}\frac{\partial \overline{u_i u_j}}{\partial x_l}, \tag{5}$$

which reduces the computational effort, but sacrifices the principle of Galilean invariance. In this expression $c_s$ has been determined to be 0.22 (Launder 1989). For the present boundary layer the measured triple correlations $\overline{u^2v}$ and $\overline{v^3}$ have been compared to estimates from equations (4) and (5) in figure 15. The estimated triple correlations depend somewhat on the method used to extract the dissipation rate

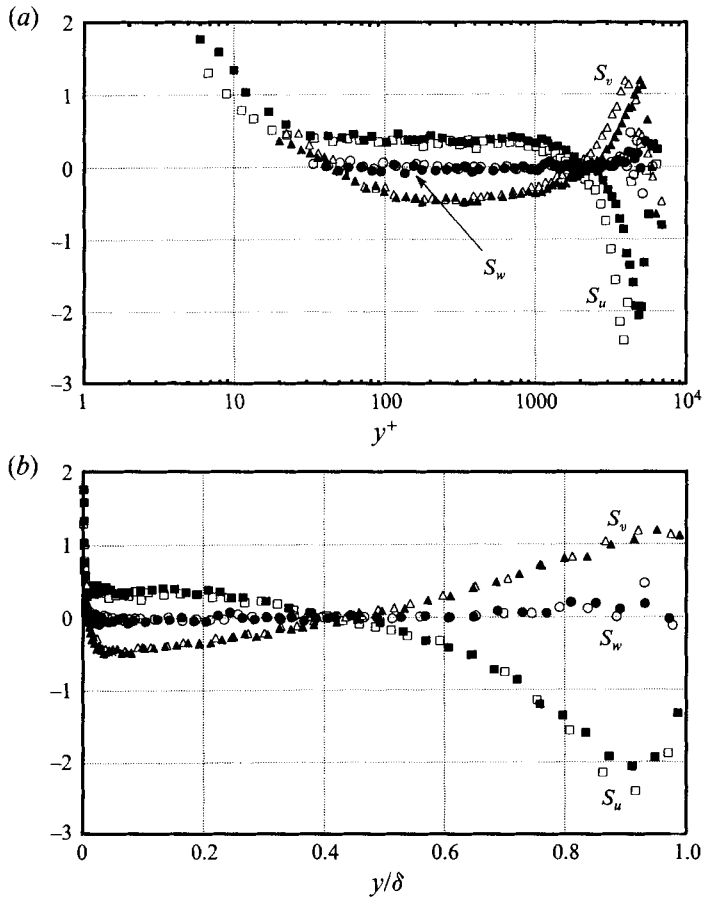


FIGURE 16. Distribution of skewness factors for $u$, $v$ and $w$ at $x = 4.0$ (open symbols) and 5.0 m (filled symbols). $u$: □, $v$: △, $w$: ○. (*a*) Inner scaling, (*b*) Outer scaling.

(equations (8) or (10)). Here dissipation from the isotropic turbulence assumption (equation (8)) was used. The agreement between the computed and measured distribution of $\overline{u^2v}$ is reasonably good using equation (4) in the outer layer, but the triple correlation is underestimated near the wall. Equation (5) is seen to represent the data well in the inner half of the layer, but overestimates the correlation by a factor of almost two further out. For the purpose of modelling the turbulent diffusion, it is the gradient with respect to $y$ rather than the actual value of the triple correlation which is important. Hence, (4) is seen to underpredict the diffusion of $\overline{u^2v}$ for $y/\delta < 0.45$, while (5) will overestimate diffusion by roughly the same factor for $y/\delta > 0.45$. For $\overline{v^3}$ the shape of the correlation is captured reasonably well showing little difference for the two equations, but the inner peak is underestimated. In the estimates of the triple correlations from (5) it was found that these correlations were completely dominated by the $y$-derivatives throughout the layer, i.e. the term $\overline{v^2}\,\partial\overline{u^2}/\partial y$ in the equation for $\overline{u^2v}$ and $\overline{v^2}\,\partial\overline{v^2}/\partial y$ in the equation for $\overline{v^3}$, respectively. The measurements show that $\overline{u^2v}$ and $\overline{v^3}$ are of the same order of magnitude. Since $\partial\overline{v^2}/\partial y$ is considerably small than $\partial\overline{u^2}/\partial y$ for most of the layer, the $\overline{u^2v}$ correlation will be overestimated in the outer layer as long as the constant of proportionality, $c_s$, is taken to be the same for both gradients.

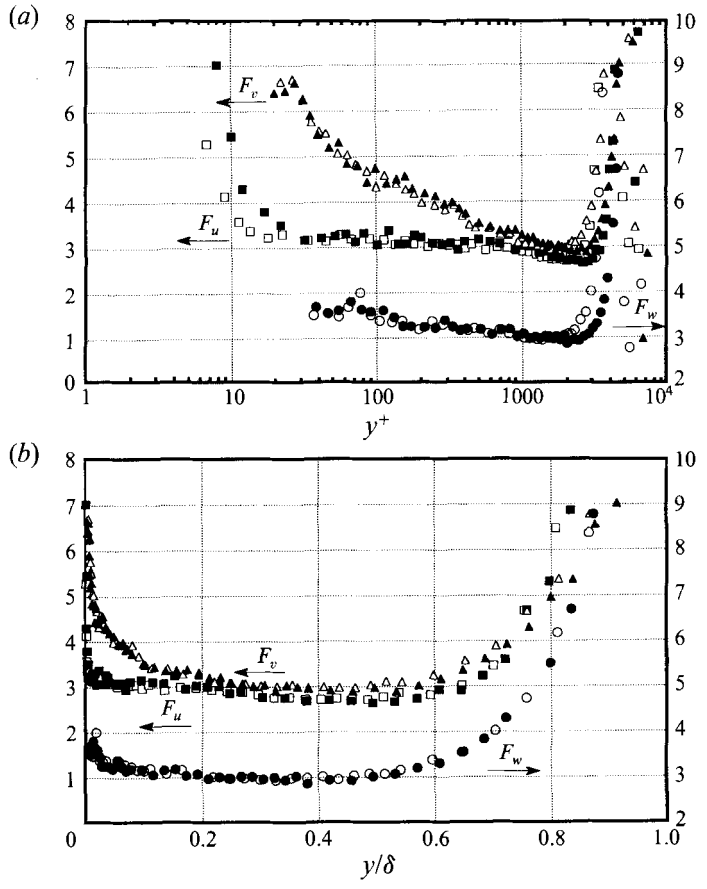


FIGURE 17. Distribution of flatness factors for $u$, $v$ and $w$. (Symbols as in figure 16.) (*a*) Inner scaling, (*b*) Outer scaling.

### 4.2. *Skewness and flatness*

The skewness and flatness factors, defined as

$$S_\alpha = \overline{\alpha^3}/(\overline{\alpha^2})^{\frac{3}{2}}, \quad F_\alpha = \overline{\alpha^4}/(\overline{\alpha^2})^2, \tag{6}$$

where $\alpha$ is one of the velocity fluctuations $u$, $v$ and $w$, respectively, have been shown in figures 16 and 17 for stations $x = 4.0$ and 5.0 m. As the distributions are similar for all the stations in the equilibrium region, only two stations have been shown. The skewness of the spanwise velocity component, $S_w$, is negligible throughout the boundary layer as a consequence of the two-dimensionality. The measurements show that this motion is close to Gaussian ($S_w \approx 0$ and $F_w \approx 3$) for most of the layer.

The skewness of the streamwise velocity component, $S_u$, is positive from the wall to the location of the maximum stresses. Here $S_u$ changes sign and becomes negative. This shows that the flow is dominated by a transport of fluid away from the outer peak in the turbulence production, although the flatness factor, $F_u$, close to 3 throughout most of the layer (figure 17) indicates important contributions from motions in the opposite direction. In the outer layer $F_v$ follows $F_u$ closely and $S_v$ is almost the reverse of $S_u$, both changing sign at the locations where the peaks in the stresses are found. The turbulent structure in the vicinity of these peaks is seen to be closely Gaussian for all normal

stresses ($S_u \approx S_v \approx S_w \approx 0$ and $F_u \approx F_v \approx F_w \approx 3$). $F_u$ falls slightly below $F_v$ and $F_w$, indicating a more narrow range of the fluctuations for $u$ than for the other turbulent velocities.

In zero pressure gradient boundary layers and channel flows $S_u$ is found to change sign at $y^+ \approx 12$ where the turbulent kinetic energy production has its maximum (e.g. Kreplin & Eckelmann 1979; Karlsson & Johansson 1988; Balint, Wallace & Vukoslavcevic 1991). $S_v$ at this point is slightly negative, but becomes positive further out ($y^+ > 30$). At the same position $F_u$ drops to a local minimum while $F_v$ reaches a maximum. This suggests a highly intermittent $v$ motion slightly biased towards strong transport of fluid towards the wall. Although measurements could not be made sufficiently close to the wall to accurately locate the peak in $F_v$, the data suggest this peak to be present at about the same $y^+$. Neither the change in sign of $S_u$ nor the minimum in $F_u$ at $y^+ \approx 12$ were found in the present flow. This indicates a significant difference in the turbulent structure owing to the pressure gradient also very close to the wall. The change in sign of $S_v$ in the present data found near $y^+ \approx 35$, from positive near the wall to negative further out, suggests that the strong diffusion from the outer production peak looses its dominance roughly at this location. However, the positive $S_u$ and the high $F_v$ values indicate strong intermittent transport towards the wall well below this point. In the zero pressure gradient layer the opposite change of sign in $S_v$ is found at roughly the same position, from negative near the wall to positive further out (Karlsson & Johansson 1989) in a region where $S_u$ is negative. The present data therefore suggest that the strong pressure gradient has reversed the dominant direction of transport close to the surface, from being away from the wall in the zero pressure gradient case, to a situation dominated by motions towards the surface. (This has been verified by a preliminary quadrant analysis (Skåre 1994) which will be reported at a later stage.)

## 5. Budgets for turbulent kinetic energy and shear stress

The transport equation for $k$ is obtained from (2). For a two-dimensional boundary layer where streamwise gradients are also important it may be written as follows:

$$\underbrace{U\frac{\partial k}{\partial x}+V\frac{\partial k}{\partial y}}_{\text{Advection}} = \underbrace{-\overline{uv}\frac{\partial U}{\partial y}+(\overline{v^2}-\overline{u^2})\frac{\partial U}{\partial x}}_{\text{Production}} \underbrace{-\frac{\partial(\overline{uk})}{\partial x}-\frac{\partial(\overline{vk})}{\partial y}}_{\text{Diffusion}} \underbrace{-\frac{1}{\rho}\frac{\partial(\overline{vp})}{\partial y}}_{pv\text{-diffusion}} \underbrace{-\frac{\mu}{\rho}\frac{\overline{\partial u_i}\,\overline{\partial u_i}}{\partial x_k\,\partial x_k}}_{\text{Dissipation}}. \tag{7}$$

The viscous diffusion terms are neglected, as their importance is restricted to the viscous region very near the wall. Only the gradient of the interaction between $p$ and the $v$ fluctuation is included, since the other gradients of the pressure–velocity interactions are assumed to be small. In the zero pressure gradient boundary layer, production and dissipation are the main contributors to the turbulent budget except near the edge of the layer (e.g. Bradshaw 1967; Spalart 1988). However, with increasing pressure gradients the advection and diffusion terms become more important.

Most of the terms in (7), have been evaluated directly from the measured data, using the profiles of the mean velocity, Reynolds stresses and triple products. The terms which could not be measured are the triple correlation $\overline{vw^2}$ and the pressure–velocity interaction contribution to the diffusion.

The production of the turbulent kinetic energy is dominated by $-\overline{uv}\,\partial U/\partial y$. Usually the second-order production term $(\overline{v^2}-\overline{u^2})\,\partial U/\partial x$ is not taken into account, but this

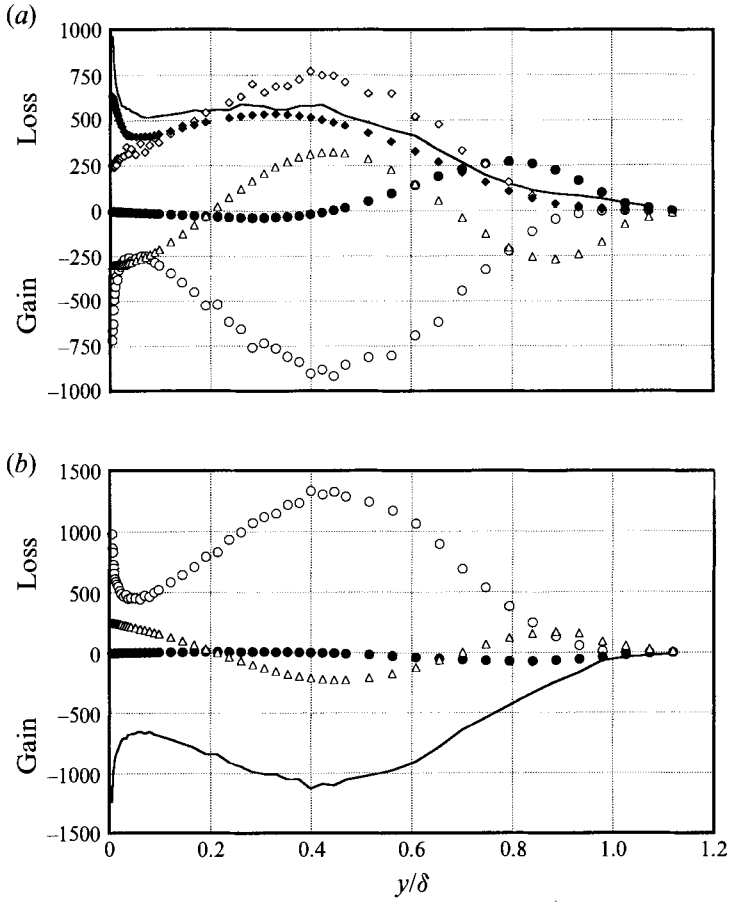


FIGURE 18. (*a*) Energy budget for the turbulent kinetic energy from data at $x = 4.4$ m. ●, advection $= \left[U\frac{\partial k}{\partial x} + V\frac{\partial k}{\partial y}\right]\frac{\delta}{u_\tau^3}$; ○, production $= \left[\overline{uv}\frac{\partial U}{\partial y} - (\overline{v^2} - \overline{u^2})\frac{\partial U}{\partial x}\right]\frac{\delta}{u_\tau^3}$; △, diffusion $= \left[\frac{\partial(\overline{uk})}{\partial x} + \frac{\partial(\overline{vk})}{\partial y}\right]\frac{\delta}{u_\tau^3}$. Dissipation rate $= \epsilon\delta/u_\tau^3$: ◆, from equation (9); ◇, from equation (10); ——, from equation (11). (*b*) Turbulent shear stress budget from data at $x = 4.4$ m. ●, advection $= \left[U\frac{\partial \overline{uv}}{\partial x} + V\frac{\partial \overline{uv}}{\partial y}\right]\frac{\delta}{u_\tau^3}$; ○, production $= \overline{v^2}\frac{\partial U}{\partial y}\frac{\delta}{u_\tau^3}$; △, diffusion $= \left[\frac{\partial \overline{u^2 v}}{\partial x} + \frac{\partial \overline{uv^2}}{\partial y}\right]\frac{\delta}{u_\tau^3}$; ——, approximate pressure–strain interaction $= \overline{\frac{p}{\rho}\left(\frac{\partial u}{\partial y} + \frac{\partial v}{\partial x}\right)}\frac{\delta}{u_\tau^3}$.

term becomes more important in flows with strong pressure gradients, since the streamwise derivatives increase. As shown in figure 9 this term contributes up to 10% of the total production in the outer part of the present boundary layer and should therefore not be neglected. The peak in $(\overline{v^2} - \overline{u^2})\partial U/\partial x$ is not coincident with the maximum shear stress, but is located further out ($y/\delta \approx 0.6$).

The most striking difference between the present flow and the zero-pressure-gradient case is that strong turbulence production does not only occur in the wall region. Considerable production is also found in the outer part of the boundary layer. As shown in figure 18 this severely affects all the terms in the turbulent energy budget.

Transport of the kinetic energy by diffusion receives its main contribution from $\partial\overline{vk}/\partial y$. However, in the present experiment $\partial\overline{uk}/\partial x$, which is normally neglected, contributes 10–15% of the total diffusion. To compute $\partial\overline{vk}/\partial y$ an estimate of the term $\overline{vw^2}$ is needed. This term may be approximated as $\overline{vw^2} = K(\overline{u^2v} + \overline{v^3})$, but as pointed out by Anderson & Eaton (1989), this tends to overestimate this correlation. This term was therefore also estimated using (5). However, the two estimates were found to be very similar and for the contribution to the turbulent budget from diffusion, no noticeable differences were found.

The diffusion process in the present experiment is split into three parts, compared to two in the zero pressure gradient case (see e.g. Townsend 1976). Energy is lost by diffusion in the domain $0.2 < y/\delta < 0.7$. As for the zero-pressure-gradient flow the diffusion brings turbulent energy towards the boundary-layer edge. However, in contrast to the zero pressure gradient case there is also a strong gain in turbulent energy owing to diffusion for $y/\delta < 0.2$.

The contribution from the pressure–velocity interaction to the diffusion process could not be obtained. Experience from DNS (e.g. Spalart 1988) indicates that this effect is of minor importance, although the effect of pressure gradients is not known. There appears, however, to be no reason to anticipate a strong sensitivity of this term to the mean pressure gradient.

The advection of kinetic energy owing to the transport by the mean flow is controlled by the two terms $U\partial k/\partial k$ and $V\partial k/\partial y$ which are of the same order of magnitude. However, the two terms have opposite signs. As for the zero pressure gradient flow, advection is only significant in the outer part of the boundary layer. In this region it is primarily balanced by the energy received by diffusion.

Most of the methods used to determine the dissipation rate rely on the assumption that the fine scale motion at high wavenumbers approaches isotropy. This leads to the following expression for the dissipation rate (e.g. Hinze 1975; Townsend 1976),

$$\epsilon = \frac{\mu}{\rho}\overline{\frac{\partial u_i}{\partial x_k}\frac{\partial u_i}{\partial x_k}} \approx 15\frac{\mu}{\rho}\overline{\left(\frac{\partial u}{\partial x}\right)^2} \approx 15\frac{\mu}{\rho}\overline{\left(\frac{1}{U}\frac{\partial u}{\partial t}\right)^2}, \tag{8}$$

where the Taylor hypothesis has been used to convert the spatial derivative to a derivative in time. Equivalently the dissipation may be obtained from the one-dimensional spectral density as

$$\epsilon \approx 15\frac{\mu}{\rho}\int_0^\infty k_1^2 E_{11}(k_1)\,\mathrm{d}k_1, \tag{9}$$

where $k_1$ is the wavenumber, $k_1 = 2\pi f/U$. The major contributions to (9) are obtained from the viscous subrange, found at the highest wave numbers. A second estimate for $\epsilon$ may be derived from the inertial subrange of the energy spectrum. In this region the following dependency exists

$$E_{11}(k_1) = Ck_1^{-\frac{5}{3}}\epsilon^{\frac{2}{3}}, \tag{10}$$

where $C$ is a constant. For boundary-layer flows Bradshaw (1967) obtained $C = 0.5 \pm 10\%$, a value which has been supported by other investigators for other types of turbulent flows (see Townsend 1976). More recently Spalart (1988) found $C \approx 0.55$ from the DNS boundary-layer data. However, Spalart points out that some Reynolds number effects may be present. In the present data the inertial subrange was easily located when plotting $k_1^{\frac{5}{3}}E_{11}(k_1)$ versus $k_1$. For most of the boundary layer this function produced a constant level in the subrange extending for more than a decade in $k_1$. This

relation also relies on the assumption of isotropy at high wavenumbers since it expresses how the turbulent kinetic energy is transferred from the large-scale motion to the scales where dissipation occurs. Since the inertial subrange is located at much lower wavenumbers, the degree of anisotropy in this range will be more pronounced and the estimates from (9) and (10) are therefore expected to be somewhat different. The differences between these estimates are expected to be largest close to the wall, owing to the strong anisotropy in this region.

Finally, the dissipation may be found as the remainder from all the other terms in the turbulent kinetic energy equation. This estimate will also include the pressure contribution to the diffusion, as well as any errors involved in the estimate of the other terms in the budget. It may therefore be less accurate than the other estimates.

$$\epsilon = U\frac{\partial k}{\partial x} + V\frac{\partial k}{\partial y} + \overline{uv}\frac{\partial U}{\partial y} + (\overline{u^2} - \overline{v^2})\frac{\partial U}{\partial x} + \frac{\partial \overline{uk}}{\partial x} + \frac{\partial \overline{vk}}{\partial y}. \tag{11}$$

It may be seen that the different methods give somewhat different results. The estimates which rely on the isotropic turbulence assumption (equations (8) or (9)) are found to be very similar to the results obtained by the difference (equation (11)), although the latter estimate is consistently higher. The ratio between these two types of estimate is nearly constant at 1.2 in the region $0.1 < y/\delta < 0.7$. The results derived from the inertial subrange are seen to reach a higher level than the other estimates in the outer region, but for $y/\delta < 0.1$ the dissipation rate is greatly underestimated.

The measurements also allowed an approximate budget for the turbulent shear stress to be computed. From (2) the following transport equation is derived:

$$\underbrace{U\frac{\partial \overline{uv}}{\partial x} + V\frac{\partial \overline{uv}}{\partial y}}_{\text{Advection}} = \underbrace{-\overline{v^2}\frac{\partial U}{\partial y}}_{\text{Production}} \underbrace{- \frac{\partial \overline{u^2 v}}{\partial x} - \frac{\partial}{\partial y}\left(\overline{uv^2} + \overline{u\frac{p}{\rho}}\right)}_{\text{Diffusion}} + \underbrace{\overline{\frac{p}{\rho}\left(\frac{\partial u}{\partial y} + \frac{\partial v}{\partial x}\right)}}_{ps\text{-interaction}} \underbrace{- \frac{\mu}{\rho}\overline{\frac{\partial u}{\partial x_k}\frac{\partial v}{\partial x_k}}}_{\text{Dissipation}}. \tag{12}$$

The viscous diffusion term has again been neglected for the same reason as given for the turbulent kinetic energy equation. The advection, production and the first two diffusion terms could be estimated directly from the measurements. The DNS simulations of Spalart (1988) have verified that the pressure diffusion and the shear stress dissipation terms are small, at least at low Reynolds numbers. The dissipation term, which vanishes for isotropic turbulence, is only effective at very high wavenumbers. Since the degree of anisotropy at the smallest scales is expected to decrease with increasing Reynolds number, the dissipation rate in the present flow is expected to play an even smaller role than in the DNS boundary layer.

The pressure–strain interaction term cannot be measured. Hinze (1975) argued that this term must be of the same order of magnitude as the production term. It must, however, be of opposite sign, since it follows from the above discussion that this is the only term in the equation which can limit the growth of $\overline{uv}$. In the budget presented in figure 18(*b*) the pressure diffusion, dissipation and pressure–strain interaction terms were grouped together, assuming that the pressure–strain term was the dominant contributor. This was obtained as the difference between the other terms in (12).

The distributions obtained for the shear stress budget resemble closely the distributions for the kinetic energy. This was expected since the dominant production terms in the two equations were found to be very similar (figure 9). However, the importance of the advection and diffusion terms in the shear stress budget is considerably reduced, implying a close balance between the production and

pressure–strain interaction terms throughout most of the layer. This agrees well with the DNS budget of Spalart (1988) for the zero-pressure-gradient boundary layer.

## 6. Conclusions

The results from an equilibrium boundary-layer experiment in a strong adverse pressure gradient have been reported. Equilibrium was obtained over a significant streamwise distance where the skin friction coefficient was maintained at a low constant level of about $C_f = 5.7 \times 10^{-4}$. In the equilibrium region, which extended for about 1.0 m, all mean velocity profiles were documented to be self-similar. It was also shown that in this region the lengthscales grow linearly with distance in accordance with the equilibrium requirements and that the non-dimensional pressure gradient, $\beta$, as well as the Clauser parameter, $G$, were constant. Townsend (1976) pointed out that equilibrium in the mean velocity may only be obtained if the turbulent stresses also show similarity. In the present experiment similarity in all the turbulent stresses as well as in the triple correlations was obtained. The gradient of the mixing length was found to increase from $\kappa_l \approx 0.41$ at the beginning of the logarithmic layer to $\kappa_l \approx 0.78$ where the layer merges with the wake. This did not influence the mean velocity profile which followed the law of the wall closely with the conventional von Kármán constant of $\kappa_u = 0.41$.

The logarithmic law of the wall may be derived assuming negligible momentum in a region of constant shear stress and a linear mixing-length distribution. Within the logarithmic layer the shear stress increased from about 1.5 to 6.5 times the shear stress at the wall in the present case. Both the difference in $\kappa$ between the mean velocity and shear stress profiles and the rapid increase in shear stress in the logarithmic layer suggests that the logarithmic layer is much more fundamental to turbulent boundary layers than just being a region of approximately constant shear stress.

The measurements showed that the ratios between the different turbulent stresses remained as for zero pressure gradient flows, indicating that the distribution of kinetic energy between the different stresses is unaffected by the pressure gradient. This was further verified by the correlation coefficient $R_{uv}$ which was found to be close to 0.42 and the structure parameter $a_1$ found to be close to 0.15 in the bulk part of the boundary layer, both values in agreement with zero-pressure-gradient flows.

The turbulence production terms showed that significant production of kinetic energy was present not only in the near-wall region, but also in the outer layer. This production in the outer layer is due to the very high turbulent shear stresses found in this region, the peak value being about sixteen times the wall stress. The peak level was found to scale linearly with the pressure gradient parameter, $\beta$. The triple correlations showed that there is a significant diffusion of energy away from this outer peak in production. In contrast to the zero-pressure-gradient boundary layer the present flow produces a strong turbulent diffusion towards the wall in the inner half part of the layer.

As a consequence of the high turbulent stresses in the outer part, high rates of dissipation were no longer limited to the wall region. In addition to the thin region near the wall where the dissipation rate is very high, considerable dissipation was found in the outer layer with a second peak close to the outer maximum in the turbulent production rate.

## REFERENCES


ANDERSON, S. D. & EATON, J. K. 1989 Reynolds stress development in pressure-driven three-dimensional turbulent boundary layers. *J. Fluid Mech.* **202**, 263–294.

BALINT, J.-L., WALLACE, J. M. & VUKOSLAVCEVIC, P. 1991 The velocity and vorticity vector fields of a turbulent boundary layer. Part 2. Statistical properties. *J. Fluid Mech.* **228**, 53–86.

BRADSHAW, P. 1967 The turbulent structure of equilibrium turbulent boundary layers. *J. Fluid Mech.* **29**, 625–645.

BROWNE, L. W. B., ANTONIA, R. A. & CHUA, L. P. 1989 Calibration of X-probes for turbulent flow measurements. *Exps Fluids* **7**, 201–208.

CLAUSER, F. H. 1954 Turbulent boundary layers in adverse pressure gradients. *J. Aero. Sci.* Feb., 91–108.

COCKRELL, D., HILL, P., LUMLEY, J., MORKOVIN, M. & EMMONS, H. 1968 Report from the evaluation committee. In *Proc. Computation of Turbulent Boundary Layers*, AFOSR-IFP-Stanford Conference (ed. S. J. Kline, M. V. Morkovin, G. Sovran & D. J. Cockrell), vol. 1, pp. 464–478.

COLES, D. E. & HIRST, E. A. 1968 Memorandum on data selection. In *Proc. Computation of Turbulent Boundary Layers*, AFOSR-IFP-Stanford Conference (ed. S. J. Kline, M. V. Morkovin, G. Sovran & D. J. Cockrell), vol. 2, pp. 47–54.

CUTLER, A. D. & JOHNSTON, J. P. 1989 The relaxation of a turbulent boundary layer in an adverse pressure gradient. *J. Fluid Mech.* **200**, 367–387.

DENGEL, P. & FERNHOLZ, H. H. 1990 An experimental investigation of an incompressible turbulent boundary layer in the vicinity of separation. *J. Fluid Mech.* **212**, 615–636.

EAST, L. F. & SAWYER, W. G. 1979 An investigation of the structure of equilibrium turbulent boundary layers. In *Turbulent Boundary Layers: Experiment Theory and Modelling*, AGARD CP-271, 6.1–6.19.

GEORGE, W. K. & CASTILLO, L. 1993 Boundary layers with pressure gradient: another look at the equilibrium boundary layer. In *Intl Conf. on Near-Wall Turbulent Flows* (ed. R. M. C. So, C. G. Speziale & B. E. Launder), pp. 901–910. Elsevier.

GLOWACKI, W. J. & CHI, S. W. 1972 Effect of pressure gradient on mixing length for equilibrium turbulent boundary layers. *AIAA paper* 72–213.

GRANVILLE, P. S. 1976 A modified law of the wake for turbulent shear layers. *J. Fluids Engng* **98**, 578–580.

GRANVILLE, P. S. 1988 Eddy viscosities and mixing lengths for turbulent boundary layers on flat plates, smooth or rough. David W. Taylor Naval Ship Research and Development Center, DTNSRDC-86–067.

GRANVILLE, P. S. 1989 A modified van Driest formula for the mixing length of turbulent boundary layers in pressure gradients. *J. Fluids Engng* **111**, 94–97.

HANJALIC, K. & LAUNDER, B. E. 1972 A Reynolds stress model of turbulence and its application to thin shear flows. *J. Fluid Mech.* **52**, 609–638.

HINZE, J. O. 1975 *Turbulence*, 2nd edn. McGraw-Hill.

KARLSSON, R. I. & JOHANSSON, T. G. 1988 LDV measurements of higher order moments of velocity fluctuations in a turbulent boundary layer. In *Laser Anemometry in Fluid Mechanics III* (ed. R. J. Adrian, T. Asanuma, D. F. G. Durao, F. Durst & J. H. Whitelaw), pp. 273–289. Ladoan-Instituto Superior Tecnico, Lisbon.

KLEBANOFF, P. S. 1955 Characteristics of turbulence in a boundary layer with zero pressure gradient. *NACA Rep.* 1247.

KREPLIN, H.-P. & ECKELMANN, H. 1979 Behaviour of the three fluctuating velocity components in the wall region of a turbulent channel flow. *Phys. Fluids* **22**, 1233–1239.

KROGSTAD, P.-Å., ANTONIA, R. A. & BROWNE, L. W. B. 1992 Comparison between rough and smooth wall turbulent boundary layers. *J. Fluid Mech.* **245**, 599–617.

KROGSTAD, P.-Å & SKÅRE, P. E. 1993 An experimental investigation of a turbulent equilibrium boundary layer near separation. In *Intl Conf. on Near-Wall Turbulent Flows* (ed. R. M. C. So, C. G. Speziale & B. E. Launder), pp. 911–920. Elsevier.

LAUNDER, B. E. 1989 Second-moment closure and its use in modelling turbulent industrial flows. *Intl J. Numer. Meth. Fluids* **9**, 963–985.

LI, J. D. & PERRY, A. E. 1989 Shear stress profiles in zero pressure gradient turbulent boundary layers. In *10th Australasian Fluid Mech. Conf.* (ed. A. E. Perry), University of Melbourne.

MELLOR, G. L. & GIBSON, D. M. 1966 Equilibrium turbulent boundary layers. *J. Fluid Mech.* **24**, 225–253.

MUSKER, A. J. 1979 Explicit expression for the smooth wall velocity distribution in a turbulent boundary layer. *AIAA J.* **17**, 655–657.

NAGANO, Y., TAGAWA, M. & TSUJI, T. 1991 Effects of adverse pressure gradients on mean flows and turbulence statistics in a boundary layer. In *8th Symp. on Turbulent Shear Flows.* Munich.

NASH, J. F. 1965 Turbulent-boundary-layer behavior and the auxiliary equation. *AGARDograph* **97**, 245–279.

OKA, S. & KOSTIC, Z. 1972 Influence of wall proximity on hot-wire velocity measurements. *DISA Information* **13**, 29–33.

PATEL, V. C. 1965 Calibration of the Preston tube and limitations on its use in pressure gradients. *J. Fluid Mech.* **23**, 185–208.

PERRY, A. E., BELL, J. B. & JOUBERT, P. N. 1966 Velocity and temperature profiles in adverse pressure gradient turbulent boundary layers. *J. Fluid Mech.* **25**, 299–320.

PERRY, A. E., LIM, K. L. & HENBEST, S. M. 1987 An experimental study of the turbulence structure in smooth- and rough-wall boundary layers. *J. Fluid Mech.* **218**, 405–438.

PERRY, A. E., MARUŠIC, I. & LI, J. D. 1993 Recent ideas and development in the modelling of wall turbulence. In *Intl Conf. on Near-Wall Turbulent Flows* (ed. R. M. C. So, C. G. Speziale & B. E. Launder), pp. 1029–1030. Elsevier.

SHILOH, K., SHIVAPRASAD, B. G. & SIMPSON, R. L. 1981 The structure of a separating turbulent boundary layer. Part 3. Transverse velocity measurements. *J. Fluid Mech.* **113**, 75–90.

SKÅRE, P. E. 1994 Experimental investigation of an equilibrium boundary layer in strong adverse pressure gradient. PhD thesis, University of Trondheim, Norway.

SPALART, P. R. 1988 Direct simulation of the turbulent boundary layer up to $Re_\theta = 1410$. *J. Fluid Mech.* **187**, 61–98.

SPALART, P. R. & LEONARD, A. 1987 Direct numerical simulation of equilibrium turbulent boundary layers. In *Turbulent Shear Flows 5* (ed. F. Durst, B. E. Launder, J. L. Lumley, F. W. Schmidt & J. H. Whitelaw), pp. 234–252. Springer.

SPALART, P. R. & WATMUFF, J. H. 1993 Experimental and numerical study of a turbulent boundary layer with pressure gradients. *J. Fluid Mech.* **249**, 337–371.

STRATFORD, B. S. 1959 An experimental flow with zero skin friction throughout its region of pressure rise. *J. Fluid Mech.* **8**, 143–155.

TOWNSEND, A. A. 1976 *The Structure of Turbulent Shear Flow*, 2nd edn. Cambridge University Press.

WILCOX, D. C. 1993 *Turbulence Modeling for CFD.* Griffin.